 CMES, vol.12, no.1, pp.1-25, 2006

On Three-dimensional Effects in Propagation of Surface-breaking Cracks

A. Dimitrov[1], **F.-G. Buchholz**[2] **and E. Schnack**[3]

Abstract: Crack propagation in 3D-structures cannot be reduced (in general) to a series of plane problems along the crack front edge, due to the existence of some "corners" on the crack front, where the elastic fields are of a real three-dimensional nature. The most important example for such a corner ist the point, where the crack front intersects a free surface of the body. According to the concept of weak and strong singularities, it is possible to obtain the asymptotics for the stress intensity factor (SIF) as well as the strain energy release rate (SERR) in the neighborhood of such a corner depending on its singular exponents, so that the convenient single parameter description on which fracture mechanics is based can be extended also to problems with corners.

Within the present work the surface-breaking crack is considered. First, the singular exponents and corresponding singular modes are calculated for arbitrarily-inclined crack geometries in order to obtain the asymptotics for the SERR from a theoretical point of view. Furthermore, detailed three-dimensional numerical results for the SERR distribution along the crack front of a single edge notched (SEN) specimen under different kind of loadings are presented in a number of case studies. And finally, related fracture experiments are discussed under special consideration of some 3D-effects near the point, where the crack front intersects the free surface.

keyword: Surface-breaking crack, corner singularity, weak and strong singularities, fracture parameter asymptotics, SEN specimen

1 Introduction

Within the framework of linear elastic fracture mechanics (LEFM) a well known methodology for characterizing the safety of structures of brittle materials containing cracks is established. In contrast to the concepts of strength of materials some fracture parameter as Irwin's stress intensity factor (SIF) k or Griffith's strain energy release rate (SERR) G are related to the material fracture toughness k_{Ic} or G_c. Because the stresses in the vicinity of a crack tip were known to be singular for a long time Westergaard (1939):

$$\sigma_{ij} = \frac{1}{\sqrt{2\pi\rho}} \left[k_I f^I_{ij}(\varphi) + k_{II} f^{II}_{ij}(\varphi) + k_{III} f^{III}_{ij}(\varphi) \right], \tag{1}$$

not the stresses themselves, but the "amplitude" of the singularity k, which depends on the loading, is defined to be the parameter controlling crack instability. ρ, φ here denotes a polar coordinate system with its origin in the crack tip, f_{ij} are the so called "angular functions", which represent the angular behavior of the stresses. It is postulated that crack propagation takes place if

$$f(k_I, k_{II}, k_{III}) > k_{Ic} \quad \text{or} \quad \sum_{i=I}^{III} G_i > G_c. \tag{2}$$

Historically this concept has been introduced for analyzing 2D crack configurations in plane strain or plain stress, which is comprehensible, since analytical solutions of elastic problems in 3D are essentially non-trivial. For instance, the SIF k_I for mode I crack opening in a simple tension far field σ_0 is determined by

$$k_I = \sigma_0 \sqrt{\pi a}\, Y, \tag{3}$$

where a denotes the crack size. The non-dimensional form-function Y has to take into account the shape of the crack. By this simple concept the processing of a wide range of plane problems is easy to handle only by evaluating Y for the actual crack configuration. Examples can be found in some stress intensity factor handbooks, see for instance Murakami (1987).

Within this context it was very natural to expect some extensions of the above technique to more realistic 3D problems. First, it has been shown (see Kassir and Sih

[1] Robert Bosch GmbH, FV/PLM2, Postfach 30 02 40, 70442 Stuttgart, Germany

[2] Institute of Applied Mechanics (FAM), University of Paderborn, Pohlweg 47-49, 33098 Paderborn, Germany

[3] Correspondence author. Institute of Solid Mechanics, University of Karlsruhe, Kaiserstr. 12, 76128 Karlsruhe, Germany, email: eckart.schnack@imf.mach.uka.de

(1975) and the references therein for an overview) that the form of stress singularity in a number of cases, including the semi-infinite plane crack, the penny-shaped crack and the elliptic crack, is covered by the plane theory, but that the stress intensity factor varies along the crack-front edge:

$$\sigma_{ij} = \frac{1}{\sqrt{2\pi\rho}} \left[k_I(s) f^I_{ij}(\varphi) + k_{II}(s) f^{II}_{ij}(\varphi) + k_{III}(s) f^{III}_{ij}(\varphi) \right], \tag{4}$$

where s denotes a coordinate characterizing the position along the crack front. In fact, this approach corresponds to a reduction of a 3D-problem to a series of 2D-problems in planes normal to the crack front edge. Therefore, a lot of important practical applications, which were amenable to the two dimensional analysis, could be solved analytically, so that the corresponding SIF distributions along the crack front were obtained in a close form for very different crack geometries and load cases Kassir and Sih (1975).

With the increasing computer power, however, the analytical approach took a back seat and was finally replaced by some numerical methods like FEM, which were apparently able to solve every imaginable problem, including some classes of surface-breaking cracks, for which analytical solutions were in general unknown. Today such numerical investigations are very popular, which leads to a constantly increasing number of publications dealing with the SIF distributions for 3D-crack problems based on the same idea as Eq. (4), see Panasyuk, Andrejkiv, and Stadnik (1981) for an overview.

Unfortunately, according to the general theory of boundary value problems in non-smooth domains Kondratiev (1967); Dauge (1988); Mazja, Nasarow, and Plamenewski (1991); Grisvard (1992); Kozlov, Maz'ya, and Rossmann (1997), see also Leguillon and Sanchez-Palencia (1987) for an excellent engineering overview, crack propagation in real 3D-structures cannot in general be reduced to a series of plane problems along the crack front edge. This technique fails due to the existence of some special "corners" on the crack front, the most important of which being the point where the crack front terminates on a boundary surface. Near this point the elastic fields are essentially of a three-dimensional nature and the plane crack tip theory does not apply. Moreover, the type of stress singularity may differ from the well known $1/\sqrt{\rho}$ behavior Bazant and Estenssoro (1979); Ghahremani (1991); Leguillon (1995); Dimitrov, Andrä, and Schnack (2001), which has the consequence that the SIFs are no longer well defined (remember that k was the amplitude of a special $1/\sqrt{\rho}$ stress singularity). The above named successful reduction of a 3D problem to the plane theory was only possible due to the fact that the crack front edge was considered as *smooth* and *far enough away* from the boundary surfaces, so that corner points were not present.

With regard to the above comments the question arises, whether it is possible to define a convenient single parameter description of the state near such a three-dimensional corner point, in analogy to the SIF in the plane case. Since the elastic fields can be expanded in the neighborhood of the corner in an asymptotical series very similar to that in the plane case, the answer is yes — it would be possible to define a corner stress intensity factor and to use it as a parameter characterizing fracture *at the corner*. However this would not be a very good idea, since a lot of corner geometries exist and it is practically impossible to perform experiments for each of them to ascertain the corresponding fracture toughness. So, the only useful strategy seems to be a further use of the well known SIF as a parameter also in the neighborhood of the corner, even if it is clear that it can be defined here only in an asymptotical sense. This assumption is by no means trivial and needs further experimental validation, of course.

However, what happens with the SIF and the SERR in the neighborhood of such a corner? From the asymptotical point of view it can be shown Dauge (2000); Leguillon and Sanchez-Palencia (1999) that both fracture parameters will have a very "simple" behavior. Depending only on the local geometry (the angle between crack-front and free surface for instance) they should tend either to infinity or to zero. An exception in form of a smooth distribution is possible only for a very specific local crack configuration. As will be shown later, this result seems to explain very well some 3D-effects detected by many numerical and experimental investigations of surface-breaking cracks Pook (1994, 1995); McKellar, Tait, and Douglas (1997); Buchholz, Wang, Lin, and Richard (1998); He and Hutchinson (2000); Dhondt, Chergui, and Buchholz (2001); Buchholz, Chergui, and Richard (2001b), which has been the main motivation for realizing the present work. On the other hand it explains also the difficulty to obtain coincident numerical results in the neighborhood of the free surface — most numerical methods have unconquerable convergence problems near points with high solution gradients, so that arbitrary results can be expected in this region, depending on the mesh size. Of course, this situation can be detected by a convergence analysis (a series of calculations on different grids), however our experience shows that such analyses are performed in very few cases. This seems to be even more important, because many numerical studies are used as a basis for empirical equations for the SIF or SERR distribution along a 3D crack front. With this in mind, numerical investigation should be treated with caution, especially in the neighborhood of corner points, as has already been noted Pook (1994).

Although the existence of points with a three dimensional stress state is well known Bazant and Estenssoro (1979); Ghahremani (1991); Leguillon (1995); Dimitrov, Andrä, and Schnack (2001), the above named consequences for the SIF and SERR distributions (and therefore for modeling crack growth in three dimensions) does not seem to be widely accepted, especially in the fracture mechanics community. In a typical work dealing with SIF or SERR calculation in 3D it is usually argued that effects of corner singularities may be neglected, since the effective zone of corner dominance is relatively small or because a high numerical accuracy at the corner is not worth pursuing (at later propagating stages the corner will exhibit the same singularity as in the plane case) or simply no attention is payed to the corner and all related effects are ignored. However, if the numerical analysis is performed on a "wrong" geometry, i.e. not exactly on one that would have a propagating crack (numerical analysis preferably deals with cracks which have a termination angle of 90° both for semi-elliptical and tunnel cracks Pook (1995)), the corner influence will still be present and will affect the accuracy of the numerical results. In a related experiment the parameter controlling fracture may tend to infinity and crack growth will take place first at the corner, *even if* its zone of influence is small. Neglecting such effects will cause a non-conservative approach.

On the other hand, many works dealing with the asymptotical investigation of singular problems in elasticity are limited to the calculation of singular exponents for different material and geometrical properties, without showing the important practical consequences. Very few references can be found in the literature with respect to the validation of the above concepts, one of them is the fundamental early work of Bazant and Estenssoro Bazant and Estenssoro (1979), however a lot of new theoretical results have been obtained in the last two decades, which will be taken into account in a current study.

In this spirit we are trying to give a more holistic picture of the 3D crack propagation under special consideration of free surface effects. We start in Section 2 with an overview of some important recent results in asymptotical expansion theory. These results are the basis for the concept of weak and strong singularities Leguillon and Sanchez-Palencia (1992), which relatively easily describes the interaction between corner and edge for a surface-breaking crack in terms of their characteristic singular exponents and allows the development of an asymptotics for SIF and SERR in the neighborhood of the boundary surface. In Section 3 a software for the calculation of the generally unknown corner singularity is presented. With the help of this technique the local problem of a surface-breaking crack is analyzed for different crack geometries and the corresponding corner singularity is calculated. In Section 4 a short overview of the modified virtual crack closure integral (MVCCI) method is given, by which the numerical calculation of the SERR distribution along the crack front edge can easily be performed in combination with the finite element method (FEM).

In Section 5, the main part of the present work, a number of case studies for different surface-breaking crack configurations is analyzed by three different techniques. First, the SERR distribution, calculated numerically by the MVCCI method on the basis of a FE-model of the problem is presented. This distribution is then compared with the asymptotical expansion of the solution, based on the results in Section 3, in order to show what should be the asymptotics of the SERR near the free surface from the theoretical point of view. And finally, corresponding fracture experiments are presented and discussed. Thus, by looking at a number of problems from three different angles it is shown that the asymptotical theory can be used to explain all discussed 3D-effects in crack propagation successfully. Moreover, it is emphasized, that some of the widely used arguments for neglecting the effect of corner singularities should be revised. A corresponding conclusion is given in Section 6.

2 Asymptotical analysis. Weak and strong singularities

2.1 Asymptotics of the stress intensity factor

Consider a crack with stress-free surfaces and a smooth crack front in a homogeneous material, Figure 1. The crack terminates in point O on the free surface. We are interested in the linear elastic solution of this problem near the crack front in the neighborhood of O.

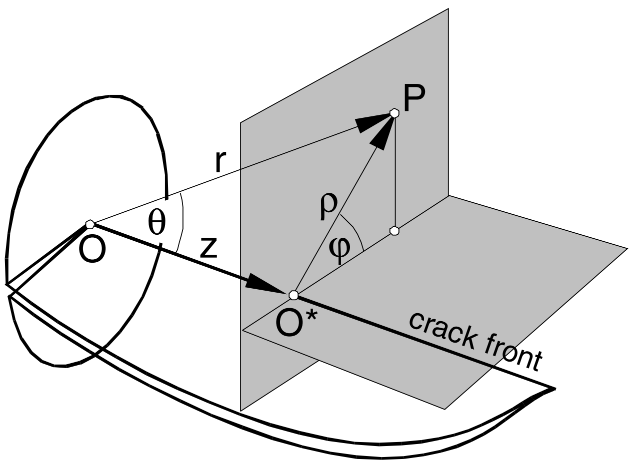

Figure 1 : Geometrical relations near the point, where a crack terminates at a stress-free boundary surface.

It is well known, see for instance Dauge (2000); Costabel, Dauge, and Duduchava (2001) and the references therein, that the displacements in a point P near the crack front can be expressed in cylindrical coordinates ρ, φ, z as an asymptotical series

$$\mathbf{u}(\rho, \varphi, z) = k(z)\, \rho^{1/2}\, \hat{\mathbf{u}}(\varphi) + \mathbf{u}_{\text{rem}}, \tag{5}$$

where the remainder $\mathbf{u}_{\text{rem}}$ is of order $O(\rho^{\xi})$, $\xi > 1/2$ and denotes some terms, which are less singular than $\rho^{1/2}$ with respect to ρ for a fixed z. Please note that in this case the asymptotics (5) is simpler than the general theory would predict and neither oscillatory nor logarithmical terms appear, see Costabel, Dauge, and Duduchava (2001). This expansion corresponds in fact to the usual plane crack-tip theory in a plane normal to the crack front at point O^* and $\rho^{1/2}$ is the well known square-root displacement behavior in radial direction. The angular behavior of $\mathbf{u}$ is represented by the so called angular functions $\hat{\mathbf{u}}(\varphi)$. However, the SIF $k(z)$ is now a function of z and depends on the position O^* on the crack front. One should be careful with $k(z)$ and $\mathbf{u}_{\text{rem}}$, because nothing is said about their behavior with respect to z and they can in particular tend to infinity for $z \to 0$, i.e. in the neighborhood of point O.

Similar to (5) there is another way to express the displacements in P as an asymptotical series, now with respect to a spherical coordinate system r, θ, φ with its origin in O, see Kondratiev (1967); Dauge (1988)[4]:

$$\mathbf{u}(r, \theta, \varphi) = K\, r^{\lambda}\, \hat{\mathbf{U}}(\theta, \varphi) + \mathbf{U}_{\text{rem}}. \tag{6}$$

Within the framework of traditionally used notions the termination point O acts as a "corner" and the crack front as an "edge". The whole domain in the neighborhood of O is viewed as a cone with one additional edge (the crack front) and a special cross-section. Within this context K denotes the corner stress intensity factor (CSIF) and λ the corner singularity, which is a generally unknown complex number. The exponent λ as well as the angular function $\hat{\mathbf{U}}$ depend only on the local geometry (crack front termination angle for instance) and not on the applied loads and can be determined with the software presented in the next section. With $\mathbf{U}_{\text{rem}}$ again some terms $O(r^{\mu}), \mu > \lambda$ are denoted, which are less singular than r^{λ} with respect to r, however one should be careful with $\hat{\mathbf{U}}$ and $\mathbf{U}_{\text{rem}}$, since nothing is said about their behavior with respect to θ and they can in particular tend to infinity for $\theta \to 0$, i.e. in the neighborhood of the crack front.

Because the expansions (5) and (6) refer to the same physical quantity it is possible to identify $k(z)$ from them. The obvious geometrical relation

$$r = \frac{z}{\cos(\theta)}, \qquad \rho = z \tan(\theta)$$

leads to

$$k(z)\, z^{1/2}\, \tan^{1/2}(\theta)\, \hat{\mathbf{u}}(\varphi) + \mathbf{u}_{\text{rem}} = K\, z^{\lambda}\, \cos^{-\lambda}(\theta)\, \hat{\mathbf{U}}(\theta, \varphi) + \mathbf{U}_{\text{rem}} \tag{7}$$

from which the leading order of $k(z)$ is found to be:

$$k(z) \sim K\, z^{\lambda - 1/2}. \tag{8}$$

As can be seen from the above equation, $\lambda = 1/2$ marks a break even point with respect to the limit of $k(z)$ for

[4] We assume that in the expansion logarithmical terms do not appear.

$z \to 0$, i.e. in the neighborhood of O. If the real part of the corner singularity $\Re(\lambda)$ is smaller than $1/2$, then the SIF $k(z)$ will tend to infinity for $z \to 0$. This case is usually denoted as "strong-singular", see Leguillon and Sanchez-Palencia (1992). If $\Re(\lambda)$ is greater than $1/2$, the SIF $k(z)$ will tend to zero for $z \to 0$ and this case is denoted as "weak-singular", see Leguillon and Sanchez-Palencia (1992). It is remarkable that this behavior depends only on the edge and corner singularity $1/2$ and λ and therefore only on the local geometry and *not* on the loading[5].

A more rigorous proof of (8) can be found in Dauge (1988, 2000), where (8) is generalized for arbitrary edge singularity, because $1/2$ is only a special case for a crack in a homogeneous body. It should also be noted that (5) and (6) are not really satisfactory from the viewpoint of asymptotical theory, since neither the edge remainder $\mathbf{u}_{\mathrm{rem}}$ nor the corner remainder $\mathbf{U}_{\mathrm{rem}}$ are really smooth, as has been mentioned, and both can blow up, either for $z \to 0$ or $\theta \to 0$. This fact was the motivation and starting point for improved (and much more complex) expansion equations with smooth remainders, see v. Petersdorff (1989); Dauge (2000), however the simple relations presented here illustrate very well the interaction between edge and corner and are therefore satisfactory for our purposes.

2.2 Asymptotics of the strain energy release rate

Similarly to the asymptotics for the SIF in the neighborhood of the corner O derived in the previous section, it is also possible to derive an asymptotics of Griffith's strain energy release rate considering a propagating crack as small perturbation of an originally cracked structure and using some tools like the matched asymptotics technique from the perturbation theory, see Leguillon and Sanchez-Palencia (1987, 1992); Leguillon (1993); Leguillon and Sanchez-Palencia (1999).

Let us again consider a crack with stress-free surfaces and smooth crack front which terminates in point O on the free surface, Figure 1. We are referring to this configuration as the unperturbed one. After the crack is propagating at O on a small distance ε (where ε denotes the dimensionless size of propagation) we obtain a configuration, which will be referred to as the perturbed one.

[5] An implicit dependence is still present: Using a special symmetrical loading it is possible to excite selective different modes with different singular behavior. This point will be discussed later.

Following Leguillon and Sanchez-Palencia (1999) two expansions[6] of the perturbed state are appropriate for obtaining the asymptotics of G: The first one (so called "outer expansion") is valid everywhere in the structure, except the vicinity of the crack extension:

$$\mathbf{u}^{\varepsilon}(\mathbf{x}) = \mathbf{U}^0(\mathbf{x}) + f_1(\varepsilon)\mathbf{U}^1(\mathbf{x}) + \ldots; \lim_{\varepsilon\to 0} f_1(\varepsilon) = 0. \tag{9}$$

The second one ("inner expansion") is defined on a domain, obtained from a small neighborhood of O after changing the variables $\mathbf{y} = \mathbf{x}/\varepsilon$ and taking the limit for $\varepsilon \to 0$, i.e. after scaling with $1/\varepsilon$. It is an unbounded domain with a crack extension equal to one.

$$\mathbf{u}^{\varepsilon}(\mathbf{y}) = F_0(\varepsilon)\mathbf{V}^0(\mathbf{y}) + F_1(\varepsilon)\mathbf{V}^1(\mathbf{y}) + \ldots; \lim_{\varepsilon\to 0} \frac{F_1(\varepsilon)}{F_0(\varepsilon)} = 0. \tag{10}$$

Such an expansion is meaningful in the vicinity of the perturbation.

Except the term $\mathbf{U}^0(\mathbf{x})$, which is the classical solution of an unperturbed crack problem

$$\mathbf{U}^0(\mathbf{x}) = K\, r^{\lambda}\hat{\mathbf{U}}(\theta,\varphi) + \ldots, \tag{11}$$

all other terms whether in the outer or inner expansion need some matching conditions to be well defined: Both expansions should coincide in an intermediate region. After identifying all terms in the outer and inner expansion Griffith's SERR for quasi-statical crack propagation can be derived as the difference in the potential energy of the unperturbed and perturbed structure per unit crack surface created, see Leguillon and Sanchez-Palencia (1999):

$$G = \lim_{\varepsilon\to 0} \frac{\delta W}{\varepsilon^2} \sim \lim_{\varepsilon\to 0} K^2\, \tilde{K}\, \varepsilon^{2\lambda-1}, \tag{12}$$

where K denotes the CSIF, $\tilde{K}$ are some coefficients, which depend only on the perturbation, λ denotes the corner singularity and ε is the size of perturbation (crack extension) in the neighborhood of the crack termination point O.

As can be seen, again $\lambda = 1/2$ is a break even point for weak ($\Re(\lambda) > 1/2$, $G \to 0$) and strong ($\Re(\lambda) < 1/2$, $G \to \infty$) singularity with respect to a propagating crack at the boundary surface, see Leguillon and Sanchez-Palencia (1992).

[6] They should not be confused with the asymptotical expansions used in the previous section.

2.3 Weak and strong singularities

It is obvious that the asymptotics for both the SIF and the SERR derived in the previous sections plays a central role for determining quasi-static crack propagation independent whatever approach (Irwin or Griffith) is used. $1/2$ marks in both asymptotics a break even point for weak ($\Re(\lambda) > 1/2, G \to 0, k \to 0$) and strong ($\Re(\lambda) < 1/2, G \to \infty, k \to \infty$) singularities, see Leguillon and Sanchez-Palencia (1992).

Let us discuss what should be the behavior of a crack with either weak or strong corner singularity at its termination point O.

If the crack configuration near O is such that $\Re(\lambda) < 1/2$, then the SERR (or the SIF) will tend to infinity[7] for $z \to 0$. Near O both the SERR and the SIF will have significant larger values than at the rest of the crack front inside the structure. Therefore a very small load will be sufficient to cause *local* crack growth near O, Figure 2a. As a consequence the crack at the boundary will propagate ahead of the crack inside and the local geometry near O (the crack front termination angle for instance) will change. In the next section we will show that this change will result in an increasing $\Re(\lambda)$ till a configuration is reached at which $\Re(\lambda) = 1/2$. From this moment the crack growth will be self-similar, so that all points on the crack front will propagate simultaneously.

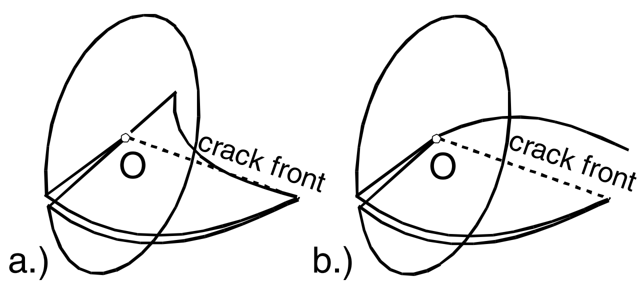

Figure 2 : Crack growth near the free surface for a.) strong and b.) weak singularity.

[7] If the parameter controlling fracture tends to infinity, then crack growth will takes place for arbitrary small loading, which is not observed. A possible solution of this problem can be found in the finite fracture mechanics, assuming that the crack increment is not arbitrarily small, but finite, see Leguillon and Sanchez-Palencia (1992). In this case the crack growth is not smooth, but takes place in small jumps and the corresponding fracture parameters are very large or very small, but finite , see Leguillon and Sanchez-Palencia (1992).

If the crack configuration near O is such that $\Re(\lambda) > 1/2$, then the SERR (or the SIF) will tend to zero for $z \to 0$. Near O both the SERR and the SIF will have significantly smaller values than the rest of the crack front inside the structure. During an increasing loading nothing will happen, till a critical state is reached, at which $G > G_c$ (or $k > k_{Ic}$) and the crack inside the structure will start to grow. This process will change the local geometry near O, so that the crack front at the boundary will stay behind the rest of the crack front, Figure 2b. In the next section we will show that this will result in a decreasing $\Re(\lambda)$ till a configuration is reached, at which the corresponding corner singularity $\Re(\lambda) = 1/2$. From this moment the crack will again propagate self-similarly.

Let us finally discuss what will happen, if for a given crack configuration near O two modes are present, a strong-singular one with $\Re(\lambda) < 1/2$ and a weak-singular one with $\Re(\lambda) > 1/2$. In this case the terms in the asymptotics of the fracture parameter associated with the strong-singular mode will tend to infinity for $z \to 0$ and those associated with the weak one will tend to zero: Crack propagation will take place for very small loads at O till a critical configuration is reached, as described above. If at this configuration the weak mode remains weak (which is the case for the surface-breaking crack, see next section, but is not necessary true in general), so that its terms in the asymptotics of the fracture parameter remain zero at the free surface, then further crack propagation in the neighborhood of O will be controlled *only* by the strong-singular mode. If the weak mode now becomes a strong one, then the dominant of both modes will control fracture in asymptotical sense, however in a finite body the other mode will play also a certain role (higher order terms, stability etc).

A consequence of this behavior is that self-similar crack propagation can take place only for special local crack geometries (termination angles), namely those at which the corner singularity is exactly $1/2$. This assumption, even if based on physical soundness, has been formulated for the first time in a fundamental paper Bazant and Estenssoro (1979) where it has been shown that the experimentally detected crack termination angle for a mode I crack has a good correlation to the theoretically expected value. In Section 5 we intend to show analogous results for inclined crack geometries and mixed mode loading. Moreover, we will show that the crack-opening modes at the free surface differ from the well known plane-strain modes I, II and III, which explain in very natural way the so called "mode coupling effect" at the free surface.

And finally, let us briefly discuss some implications of above results to the mixed-mode growth of fatigue cracks. In the case when $\Re(\lambda) > 1/2$ the SERR (or the SIF) will tend to zero at $z \to 0$ for *any* load, as already mentioned. That means, the SERR- or SIF-*range* will have a significantly smaller value at the free surface than at the rest of the crack front inside the structure. During an increasing load range the crack inside the structure will start to grow if $\Delta k > \Delta k_{th}$. This again will change the local geometry near O, so that a configuration will be reached, at which $\Re(\lambda) = 1/2$ and the further fatigue crack growth will be self-similar.

In the case when $\Re(\lambda) < 1/2$ the SERR (or the SIF) will tend to infinity (or will be finite, but very large) at $z \to 0$ again for *any* load. Near O both the SERR and the SIF will have significant larger values than k_{Ic} or G_c even if the load level is small, which will be sufficient to cause *local quasi-static* crack growth near O before the SIF-range inside the structure reaches Δk_{th}. As a consequence the crack at the boundary will propagate ahead of the crack inside, as already mentioned, till a configuration is reached at which $\Re(\lambda) = 1/2$. Fatigue crack growth will now take place if $\Delta k > \Delta k_{th}$.

3 Corner singularities in 3D elasticity

From a theoretical point of view it is well known that the linear elastic solution may contain gradient singularities, if the domain of consideration includes re-entrant corners like cracks or sudden changes in the material properties as in the case of composites, see for example Kondratiev (1967); Dauge (1988); Mazja, Nasarow, and Plamenewski (1991); Grisvard (1992); Kozlov, Maz'ya, and Rossmann (1997); Leguillon and Sanchez-Palencia (1987) and the references therein for an overview. For the treatment of such situations it can be helpful to expand the solution in the neighborhood of the singular point in an asymptotical series

$$\mathbf{u} = \sum_i K_i\, r^{\lambda_i}\ \hat{\mathbf{U}}_i(\theta, \varphi), \tag{13}$$

where r, θ, φ are the spherical coordinates, λ_i are the singularity exponents, K_i the corner SIFs (CSIF) and $\hat{\mathbf{U}}_i$ are the so called "angular functions".

The asymptotical series (13) can be explicitly constructed, particularly if one considers special geometries and material properties, see Williams (1957); Kassir and Sih (1975). In this case the exponents λ_i are obtained as solutions of some transcendent equations. However, for general three-dimensional problems such approaches do not work and some numerical methods are needed to obtain λ_i and $\hat{\mathbf{U}}_i$. We will now briefly describe a technique introduced in a previous work Dimitrov, Andrä, and Schnack (2001); Dimitrov and Schnack (2002) for isotropic problems and extended in Dimitrov, Andrä, and Schnack (2002) to anisotropic material properties. It is based on a weak formulation and a finite element approximation technique and results in a quadratic eigenvalue problem, which is solved iteratively. A detailed description as well as an overview of some other techniques can be found in Dimitrov, Andrä, and Schnack (2001); Dimitrov and Schnack (2002).

3.1 Numerical method

In order to keep our considerations sufficiently general, we introduce an abstract mixed boundary value problem of linear elasticity in a bounded domain $\Omega \subset \mathbb{R}^3$ which coincides with a cone $\mathcal{K}$ in the ε-vicinity U_O^ε of the origin O, so that $\Omega_O^\varepsilon := \mathcal{K} \cap U_O^\varepsilon = \Omega \cap U_O^\varepsilon$, see Figure 3. We denote with S the cross-section of the cone on the unit sphere. By this general model every geometry containing a conical singular point can be described (note that the shape of S is not specified), including the problem of a surface breaking crack.

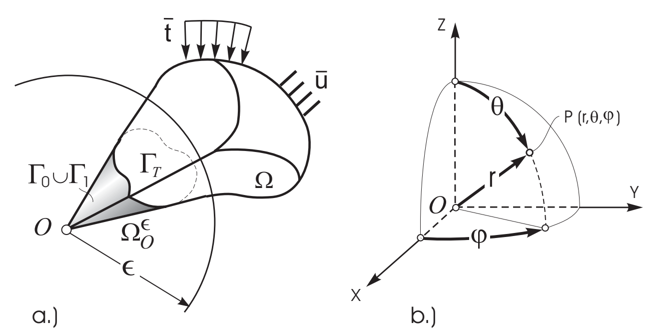

Figure 3 : a.) Boundary value problem with a singular point O. b.) Spherical and Cartesian coordinate systems in O.

Our aim is to find all solutions, often called the *eigenstates*, which satisfy the differential equation of elasticity and the boundary conditions in a sufficiently small neighborhood Ω_O^ε of O, i.e. on $\Gamma_0 \cup \Gamma_1$, but not the boundary conditions remote from O, i.e. on Γ_T. By $\Gamma_0, \Gamma_1, \Gamma_T$ the Dirichlet, Neumann and transmissional part of the boundary $\partial\Omega_O^\varepsilon$ respectively are denoted. We obtain the eigenstates by solving the Lamé system on Ω_O^ε with *only* the local boundary conditions,

$$\begin{aligned} &\mathcal{L}\mathbf{u} := \mathcal{D}^T \mathbf{C}\, \mathcal{D}\, \mathbf{u} = \mathbf{0} \quad \text{on } \Omega_O^\varepsilon, \\ &\mathbf{u} = \mathbf{0} \quad \text{on } \Gamma_0, \\ &\mathcal{T}\mathbf{u} := \mathbf{t}(\mathbf{u}) = \mathbf{0} \quad \text{on } \Gamma_1, \end{aligned} \tag{14}$$

where $\mathcal{D}(\partial_x, \partial_y, \partial_z)$ is the symmetrical gradient operator in matrix notation, $\mathbf{C}$ denotes the matrix of elastic moduli and $\mathbf{t}$ are the boundary tractions. In other words we consider a local problem with zero body forces and homogeneous boundary conditions.

Because (14) is not a *full* boundary value problem (there are no conditions on a part of the boundary Γ_T, i.e. we consider the solution itself as boundary condition on Γ_T), the requirements of the uniqueness-theorem are not fulfilled and the solution is therefore non-unique. We obtain a set of solutions from which we should exclude these with unbounded elastic energy: We only look for solutions in the Sobolev space $[H^1(\Omega_O^\varepsilon)]^3$ in order to have a square-integrable first derivative[8]. The unique solution of the problem in the vicinity of O can be obtained afterwards as a linear combination of all eigenstates, so that *all* boundary conditions including the transmissional one on Γ_T are fulfilled.

Since we are interested in a numerical solution, the boundary value problem (14) should be formulated in a weak form. Let us denote the space of admissible (with respect to the boundary conditions) displacement fields by $[H_0^1(\Omega_O^\varepsilon)]^3$. Then, introducing some test function $\mathbf{v} \in [H_0^1(\Omega_O^\varepsilon)]^3$, we formulate

Problem 1 *Find* $\mathbf{u} \in [H^1(\Omega_O^\varepsilon)]^3$*, so that*

$$\mathcal{B}(\mathbf{u}, \mathbf{v}) = 0, \quad \forall \mathbf{v} \in [H_0^1(\Omega_O^\varepsilon)]^3, \tag{15}$$

where the bilinear form $\mathcal{B}(\mathbf{u}, \mathbf{v})$ *is defined in the linear elasticity by*

$$\mathcal{B}(\mathbf{u}, \mathbf{v}) := \int_{\Omega_O^\varepsilon} \boldsymbol{\sigma}^T(\mathbf{u})\, \boldsymbol{\varepsilon}(\mathbf{v})\, d\Omega. \tag{16}$$

The r.h.s. in (15) vanishes because of the homogeneous boundary conditions. The stress and strain vectors, which contain all independent components of the stress and strain tensors respectively, are defined by

$$\begin{aligned} \boldsymbol{\varepsilon}^T &:= [\varepsilon_x, \varepsilon_y, \varepsilon_z, 2\varepsilon_{xy}, 2\varepsilon_{xz}, 2\varepsilon_{yz}], \\ \boldsymbol{\sigma}^T &:= [\sigma_x, \sigma_y, \sigma_z, \tau_{xy}, \tau_{xz}, \tau_{yz}]. \end{aligned} \tag{17}$$

We now consider a finite-element approximation of the weak problem (15). Introducing two different finite-dimensional subspaces $U_h \neq V_h$ as trial and test spaces we obtain

Problem 2 *Find an approximate solution* $\mathbf{u}^h \in U_h \subset [H^1(\Omega_O^\varepsilon)]^3$*, so that*

$$\mathcal{B}(\mathbf{u}^h, \mathbf{v}^h) = 0, \quad \forall \mathbf{v}^h \in V_h \subset [H_0^1(\Omega_O^\varepsilon)]^3. \tag{18}$$

Such a scheme is called *Galerkin-Petrov method*.

Concretely, the spaces U_h, V_h are obtained by the triangulation of S into triangles Δ_i. According to (13) the trial and test functions in a typical space sector $(r, \theta, \varphi) \in [0, \varepsilon] \times \Delta_i$ can be expressed by

$$\mathbf{u}_i^h(r, \theta, \varphi) = r^\lambda \mathbf{N}(\theta, \varphi)\, \mathbf{d}_i, \tag{19}$$

$$\mathbf{v}_i^h(r, \theta, \varphi) = \Phi(r)\, \mathbf{N}(\theta, \varphi)\, \mathbf{b}_i, \tag{20}$$

where the matrix $\mathbf{N}$ collects the shape functions of the approximation and $\mathbf{d}_i$ denotes the nodal displacement vector, see Dimitrov and Schnack (2002).

Equation (19) is the main idea of this method: By a semi-continuous approach, in which the discretization is performed only in θ, φ, a separation of variables can be enforced, so that the final problem is independent of r.

Introducing (19) in the expression for the discrete bilinear form (18) and assuming the constitutive relation $\boldsymbol{\sigma}(\mathbf{u}_i^h) = \mathbf{C}\, \boldsymbol{\varepsilon}(\mathbf{u}_i^h)$ we obtain after some additional transformations and the substitution $\lambda = \overline{\lambda} - 1/2$ a quadratic eigenvalue problem

$$\left[\mathbf{P} + \overline{\lambda}\mathbf{Q} + \overline{\lambda}^2\mathbf{R}\right] \mathbf{d} = \mathbf{0}. \tag{21}$$

The definition of the material matrix $\mathbf{C}$ for different material models can be found in Dimitrov, Andrä, and Schnack (2002), the matrices $\mathbf{P}, \mathbf{Q}$ and $\mathbf{R}$ are defined in Dimitrov, Andrä, and Schnack (2001); Dimitrov and Schnack (2002). From this eigenvalue problem the singular exponents λ_i can be calculated as eigenvalues and the angular functions $\hat{\mathbf{U}}_i$ as eigenvectors. The corresponding linear eigenvalue problem is not symmetric, see Dimitrov, Andrä, and Schnack (2001), thus complex

[8] We denote by $[H^m(\Omega)]^3$ the usual Sobolev space of order m in three dimensions over a domain Ω.

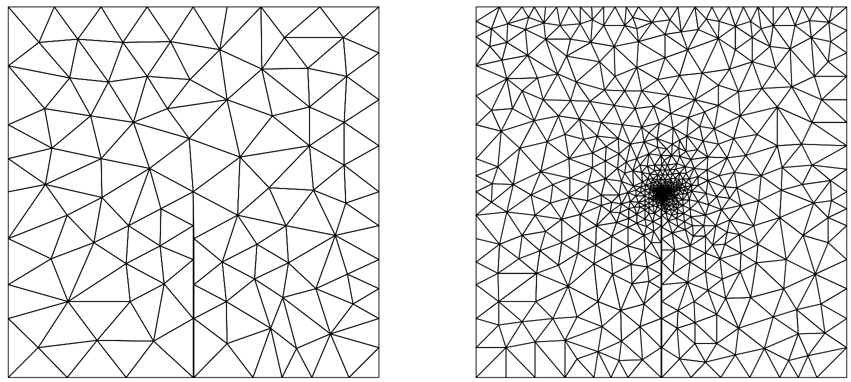

Figure 4 : Initial and final mesh used to obtain the results in Table 1 after adaptive mesh refinement.

roots are possible. Since there is no a-priori information about real or complex roots the numerical scheme always searches for complex values. In the most general case the eigenvalues may also be defective, i.e. the algebraical and the geometrical multiplicities may not coincide and some logarithmical terms can appear in the solution, which will be slightly more singular than the numerical approximation.

A suitable solution technique for (21), based on a linearization procedure and an iterative Arnoldi solver, has been proposed in a previous work Dimitrov, Andrä, and Schnack (2001); Dimitrov and Schnack (2002). It is most appropriate for large structured matrices because it requires only $2n \cdot O(k) + O(k^2)$ storage ($k \ll n$, n denotes the dimension of $\mathbf{P}, \mathbf{Q}, \mathbf{R}$) and no explicit knowledge of the corresponding standard eigenvalue problem. So the present method requires only *one* direct factorization of the matrix $\mathbf{P}$ for relatively small systems or an incomplete factorization of $\mathbf{P}$ for large systems, as well as few matrix-vector products with $\mathbf{Q}, \mathbf{R}$ in both cases to find *all* eigenvalues $\Re(\lambda) \in (-0.5, 1.0)$ as well as the corresponding eigenvectors simultaneously. The interval of interest $(-0.5, 1.0)$ is obvious, due to the restriction, that we are only interested in solutions with finite energy ($\Re(\lambda) > -0.5$) which have gradient singularity ($\Re(\lambda) < 1.0$).

Let us finally note that in the cases in which the cone cross-section contains corners a suitable mesh refinement strategy based on error control should be applied in order to obtain sufficiently accurate results. A corresponding *a-posteriori* error estimator and an adaptive scheme for mesh refinement has been proposed in Dimitrov and Schnack (2002).

3.2 Singular exponents for the surface-crack problem

With the help of the numerical method presented in the previous Section the problem of a surface breaking crack with an arbitrarily inclined crack-plane (characterized by the angle β between crack plane and free surface) and arbitrarily inclined crack front within the crack-plane (characterized by the angle α) has been analyzed, as shown in Figure 5.

The corresponding part of the unit sphere, which has to be discretized in the θ, φ space, is $(\theta, \varphi) \in \{(0, \pi/2) \times (0, \pi)\} \setminus \{(0, \alpha) \times \beta\}$. The crack surfaces are considered to be free at $(\theta, \varphi) \in (0, \alpha) \times \beta$. The calculations have been performed with quadratic sub-parametric triangular elements and adaptive mesh refinement, so that the error in the energy norm is smaller than 1%. The results for the exponents λ after mesh refinement in the case $\alpha = \pi/2, \beta = \pi/2, \nu = 0.3$ are given in Table 1.

Table 1 : Smallest singularity exponent λ and corresponding relative error for the surface-breaking crack with $\alpha = \beta = \pi/2$ after adaptive mesh refinement. Poisson's ratio $\nu = 0.3$

DOF	λ	$\Vert \mathbf{u} - \mathbf{u}^h \Vert / \Vert \mathbf{u} \Vert$
1125	0.4028	1.08e-01
2178	0.3956	5.57e-02
3711	0.3936	2.86e-02
5568	0.3930	1.42e-02
9294	0.3929	6.63e-03

It seems that the 1 % error leads to three exact significant digits for λ, which is enough for our proposes. The corresponding coarsest and finest meshes are given in Figure 4. As can be expected, within few refinement steps a strong mesh concentration near the crack front edge is obtained.

The exponents for the whole range $(\alpha,\beta) \in (\pi/40, 38\pi/40) \times (\pi/40, 20\pi/40)$ for $\nu = 0.3$ are obtained in similar calculations with a sampling step $\pi/40 = 4.5°$. Selected results are shown in Figure 5. As can be seen, up to four different modes occur, which are denoted as mode $I^* - IV^*$, so that mode I^* corresponds to the smallest eigenvalue $\Re(\lambda)$ etc. The exponents for mode I^*, II^* are real in the whole region for α, β, except for large α, where two complex conjugate exponents with the same real part exist. The corresponding imaginary part is shown in the lower right corner of Figure 5 top. Modes III^*, IV^* are present only for $\alpha > \alpha_0(\beta)$. For small β the singular exponents are two complex conjugate values with the same real part, the imaginary part is shown in the lower right corner in Figure 5 bottom. The corresponding real-part curve of these two complex exponents splits at a certain angle $\alpha_1(\beta)$, so that for $\alpha > \alpha_1$ two different real exponents appear. For large β the corresponding split takes place for $\lambda > 1.0$, which is outside the interval of interest and therefore only one real part is shown in Figure 5.

As has been noted in the previous section, the termination angle α of the crack front at the free surface for which $\lambda = 0.5$ has a special importance as the break even point between the weak and strong singularities. This critical angle depends on the material parameter ν and the inclination of the crack plane β. For $\nu = 0.3$ the critical angle has been calculated for all inclined crack planes by linear interpolation from the original data, see the results in Figure 6. As can be seen from Figure 5 there

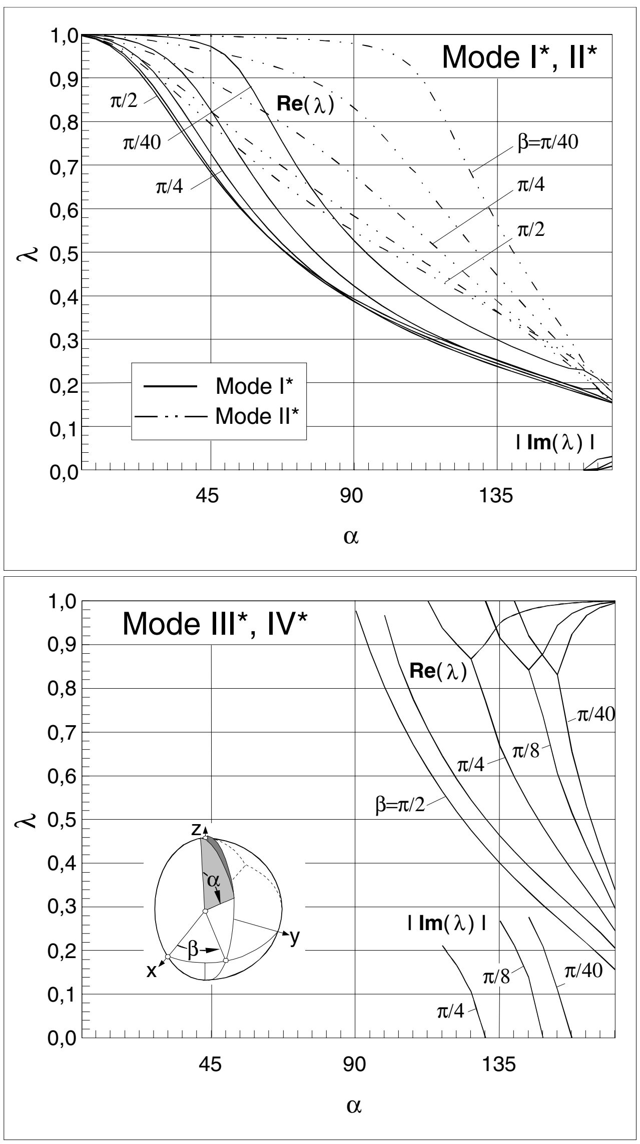

Figure 5 : Singularity exponents λ for the inclined surface-breaking crack problem. Selected results for $40\beta/\pi = 1, 5, 10, 15, 20$ and $\alpha \in (\pi/40, 38\pi/40)$. Poisson ratio $\nu = 0.3$.

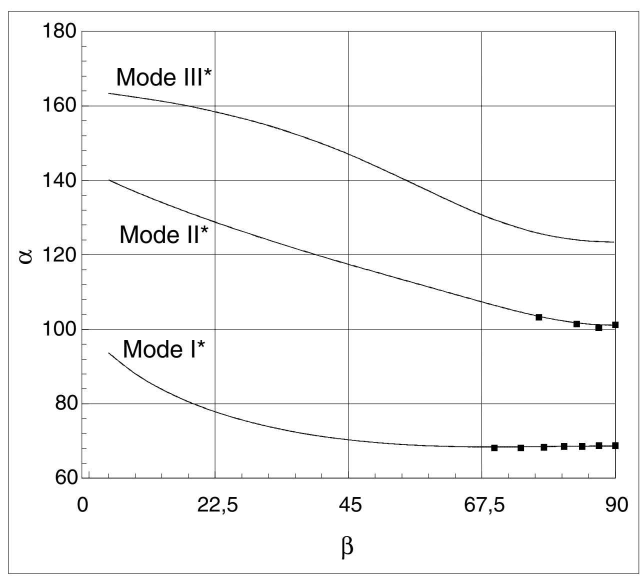

Figure 6 : Critical crack front termination angles α, for which $\lambda = 0.5$, depending on the crack plane inclination β. Poisson's ratio $\nu = 0.3$. The reference solution (small squares) is Bazant and Estenssoro (1979).

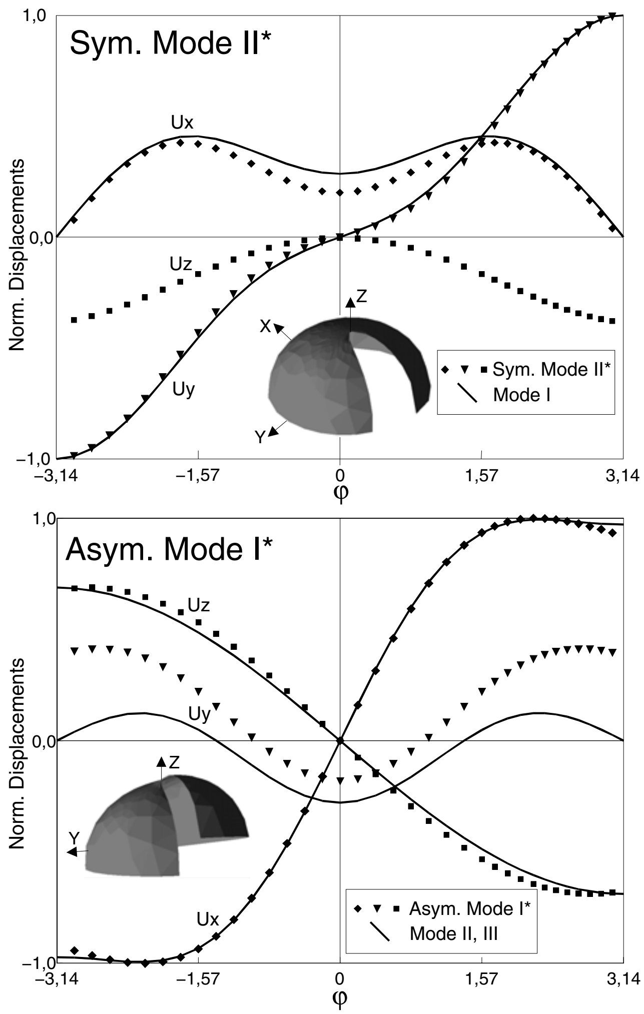

Figure 7 : Comparison between the first two space modes of a surface-breaking crack problem ($\alpha = \beta = \pi/2, \nu = 0.3$) with the modes I,II,III well known from the plane strain theory. The displacements U_x, U_y, U_z represent the trace of the space mode on the *x-y* plane (here the free surface). All displacements are normalized by the corresponding maximal value. The ratio k_{III}/k_{II} of the used normalization factors is 0.5.

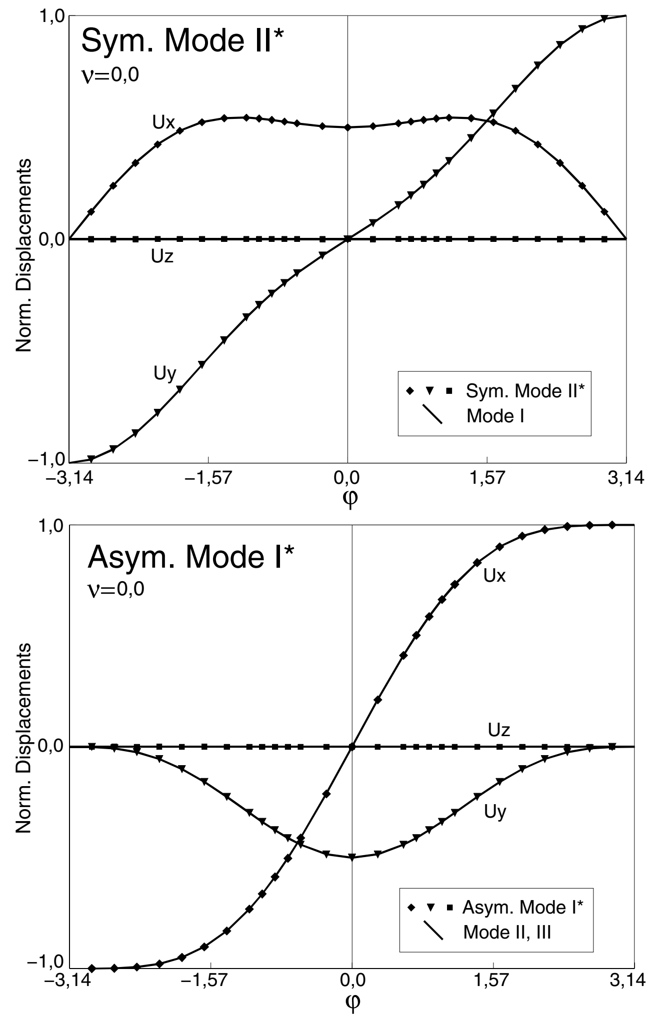

Figure 8 : Comparison between the first two modes of a surface-breaking crack problem ($\alpha = \beta = \pi/2$) with the modes I,II,III well known from the plane strain theory for Poisson's ration $\nu = 0.0$. The displacements U_x, U_y, U_z represent the trace of the space mode on the *x-y* plane (here the free surface). All displacements are normalized by the corresponding maximal value.

is no pronounced curvature of the graphs in the region $\Re(\lambda) \approx 0.5$ and the results are expected to be accurate enough. A comparison with the only other data published in the literature in Bazant and Estenssoro (1979) shows a good agreement, see the small rectangles in Figure 6. It is notable that the curves do not intersect, which means that crack propagation at the corner is always controlled by the most singular mode excited by a given loading, which is in general mode I^*.

Since the modes $I^* - IV^*$ represent a three-dimensional state, they differ from the well known plane modes I,II,III and should not be confused with them. Even if this seems to be obvious, in the literature sometimes the state at the free surface is denoted as plane stress. However, the plane stress state is *not* a limiting case of a three-dimensional solution with or without a crack (in contrast to the plane strain state), since it violates the 3D compatibility condition, as has been noted in Sih (1971). More-

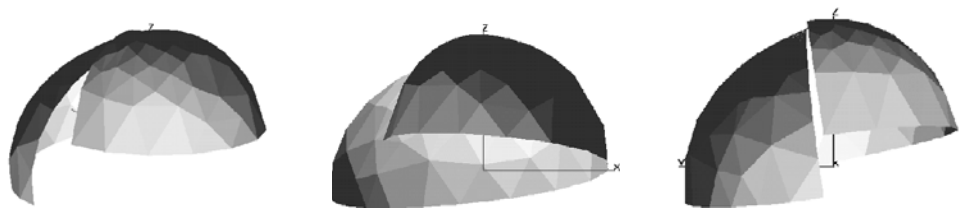

Figure 9 : Mode III^* with $\lambda_{III^*} = 0.731$ for a surface-breaking crack problem ($\alpha = \pi/2, \beta = \pi/2$). Poisson's ratio $\nu = 0.0$. The crack-opening space mode III^* is shown from different viewpoints.

over, in problems with surface cracks this state leads to unbounded displacements in the direction normal to the free surface, see Sih (1971), which is meaningless.

The state at the free surface cannot also be plain strain or a combination of the plane strain modes I,II,III, since for general angles α, β there is no corresponding symmetry with respect to which one could compare the space modes $I^* - IV^*$ with the plane strain modes I,II,III (remember that mode I,II,III are defined as symmetrical or anti-symmetrical with respect to the crack plane and a plane normal to the crack front).

Analogous symmetry only exists for the case $\alpha = \pi/2, \beta = \pi/2$, however Figure 7 shows that even in this case the symmetrical mode II^* does *not* coincide with the symmetrical mode I: The jump in U_y over the crack faces suggests a mode-I-like behavior, however due to the Poisson ratio there is an out-of-plane displacement U_z which is not present in mode I. Both modes only coincide at the free surface for $\nu = 0.0, \alpha = \pi/2, \beta = \pi/2$, see Figure 8.

Another widely used opinion refers to mode I^* as a combination of modes II,III — the so called "mode coupling effect" at the free surface. However, this could be true again only in the case $\alpha = \pi/2, \beta = \pi/2$, since for other angles no corresponding symmetry exists to compare mode I^* with the two anti-symmetrical (with respect to the crack plane) modes II,III. Figure 7 however shows that even for $\alpha = \pi/2, \beta = \pi/2$ this is not the case — for mode I^* there is a U_y displacement, which is not zero at the crack faces, in contrast to mode II, even if the jump in U_z and U_x suggest a combination of mode II and III. This effect is again related to the Poisson's ratio and vanishes for $\nu = 0.0$, see Figure 8. It is only in this case that mode I^* and mode II coincide. The situation for mode III^* is a little bit different — it is interesting to note that it does *not* correspond to the plane strain mode III, even for the case $\nu = 0.0$, see Figure 9.

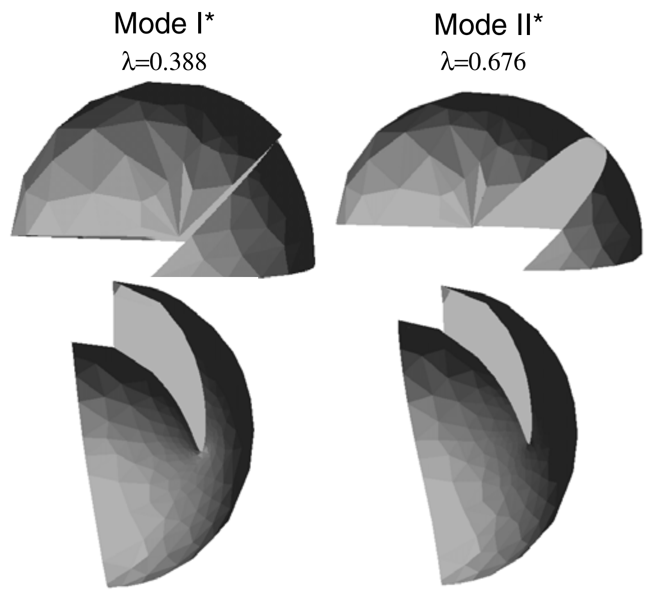

Figure 10 : The first two space modes for an inclined surface crack problem with $\alpha = \pi/2, \beta = \pi/4, \nu = 0.3$. The crack-opening modes are shown from different viewpoints.

And finally, as has been mentioned, for $\alpha \neq \pi/2, \beta \neq \pi/2$ there is no symmetry, with respect to which one could compare the corresponding modes with the plane strain modes I,II,III. For instance, in Figure 10 the two modes for $\alpha = \pi/2, \beta = \pi/4$ are shown: due to the simultaneous jump in U_x, U_y, U_z over the crack faces at the free surface a "combination" of all three modes I,II,III is suggested.

In view of the comments just made, it seems to be incorrect to refer to the state at the free surface as plane stress or plane strain or a combination of modes I,II,III and to ask (as is often done) for a limiting ratio $K_I : K_{II} : K_{III}$ at the surface. The modes $I^* - IV^*$ are independent and represent the angular part of the three dimensional state in the neighborhood of the termination point.

4 The virtual crack closure integral (VCCI) method

4.1 VCCI or 2C-Method

For the fracture analysis of a mode I crack problem, Irwin's well known analytical crack closure integral relation (see Irwin (1957)) can be written in the following FE-representation, see Buchholz (1984); Krishnamurthy, Rammamurthy, Vijayakumar, and Dattaguru (1985):

$$G_I^{2C}\left(a+\frac{\Delta a}{2}\right)=\frac{1}{t\Delta a}\,W^y,$$
$$W^y=\frac{1}{2}\,F_{y,i}(a)\,\Delta u_{y,j-1}(a+\Delta a), \tag{22}$$

which is holding for an FE-discretization as given in Figure 11.

By Eq. (22), in which t denotes the thickness of the specimen, the strain energy release rate G_I is calculated on the basis of the work to be done by the nodal point force $F_{y,i}(a)$ against the relative nodal point displacement $\Delta u_{y,j-1}(a+\Delta a)$ in order to close the crack by Δa again (Figure 11a). By Eq. (22) the numerical VCCI-method is defined for a 2D crack problem under mode I. It will be shown that by this method, which can be classified as a local energy approach, good results are obtained even for non-singular, low order standard elements and rather coarse FE-meshes, if the layout of the mesh around the crack tip is homogeneous.

The VCCI-method is also named and marked as the 2C-method (2 calculations), because two FE-analyses of the model have to be performed for the crack lengths a and $a+\Delta a$ in order to compute one SERR result $G^{2C}(a+\Delta a/2)$ as the mean value in the interval of the finite crack extension Δa. But with respect to this effort it should be emphasized that by Eq. (22) the SERR is computed numerically exactly for the actual FE discretization under consideration, even for finite crack extensions $\Delta a >> 0$. On that account no term $\lim \Delta a \to 0$ is expressed in Eq. (22) and the notation $G^{2C}(a+\Delta a/2)$ stresses its meaning as the mean value of the SERR in the interval Δa of the finite crack extension, which has to be correlated to $a+\Delta a/2$, the corresponding mean value of the crack length in the interval under consideration.

4.2 MVCCI or 1C-Method

Rybicki and Kanninen Rybicki and Kanninen (1977) have introduced the modified virtual crack closure integral (MVCCI) method in order to avoid the additional effort of a second FE-analysis for an extended crack of length $a+\Delta a$, respectively. This can be achieved if, with reference to Eq. (22) and to Figure 11a, the required relative nodal point displacement $\Delta u_{y,j-1}(a+\Delta a)$ from the extended crack is replaced by the corresponding relative nodal point displacement $\Delta u_{y,i-1}(a)$ of the original crack with crack length a. By this numerically highly effective MVCCI or 1C-method (1 calculation) the SERR is calculated by

$$G_I^{1C}(a)=\lim_{\Delta a\to 0}\frac{1}{t\Delta a}\,W^y,$$
$$W^y=\frac{1}{2}\,F_{y,i}(a)\,\Delta u_{y,i-1}(a). \tag{23}$$

The assumptions under which Eq. (23) is holding are the same as for Eq. (22). The term $\lim \Delta a \to 0$ in Eq. (23) expresses that the MVCCI or 1C-method is an approximate approach, with convergence to the exact solution only for $\Delta a \to 0$. However, it has been shown in Rybicki and Kanninen (1977) that for small Δa also a good accuracy can be achieved.

In the case of in-plane mixed mode loading conditions at the crack tip or in the 3D-case including out-of-plane shear the additional mode II or mode III SERRs can be obtained readily by substituting the relevant x- and z-components of the nodal point forces and the relative nodal point displacements into Eq. (23). The total SERR at the crack tip or at a nodal point located along the crack front is then defined by

$$G_T^{1C}(a)=\sum_i G_i^{1C}(a), \quad i=I,II,III. \tag{24}$$

Thus, the numerically highly effective MVCCI-method for 2D-fracture analysis can be generalized in conjunction with standard low order volume element discretizations in a rather straight-forward way in order to cover also complex 3D-fracture problems. First, Eqs. (22)-(24) have to be evaluated at all nodal point positions $k=1,2,\ldots$ along the crack front (Figure 11b) and they have to be interpreted there with respect to a locally defined crack front coordinate system, respectively. Second, the constant thickness t at the 2D-problems has to be replaced by an effective thickness Δt_k, which is correlated to the nodal point position k under consideration and evaluation (Figure 11). The resulting formulae with reference to Buchholz, Grebner, Dreyer, and Krome

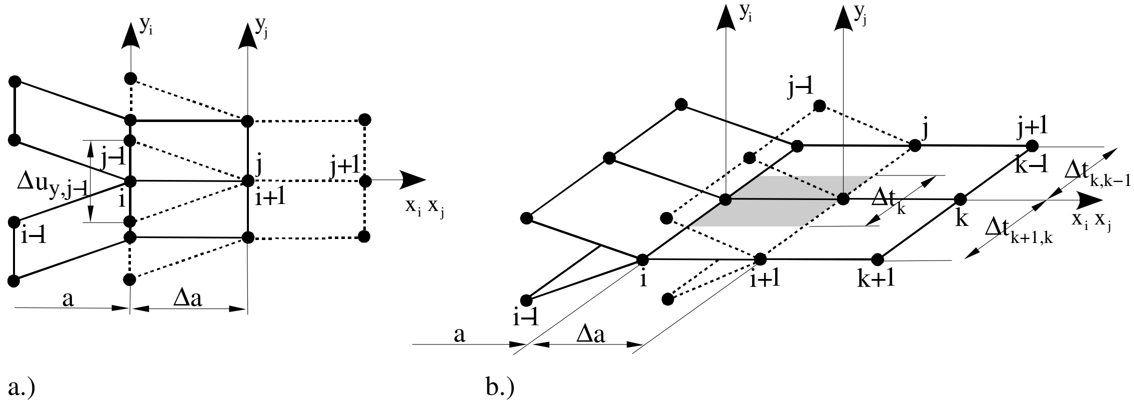

Figure 11 : Computational VCCI-methods a.) for 2D and b.) for 3D finite element discretizations.

(1988) are

$$
\begin{aligned}
G_I^{1C}(a,\Delta t_k)_k &= \lim_{\Delta a\to 0} \frac{1}{\Delta t_k\,\Delta a}\, W_k^y, \\
W_k^y &= \frac{1}{2}\,\left(F_{y,i}(a)\,\Delta u_{y,i-1}(a)\right)_k, \\
G_{II}^{1C}(a,\Delta t_k)_k &= \lim_{\Delta a\to 0} \frac{1}{\Delta t_k\,\Delta a}\, W_k^x, \\
W_k^x &= \frac{1}{2}\,\left(F_{x,i}(a)\,\Delta u_{x,i-1}(a)\right)_k, \\
G_{III}^{1C}(a,\Delta t_k)_k &= \lim_{\Delta a\to 0} \frac{1}{\Delta t_k\,\Delta a}\, W_k^z, \\
W_k^z &= \frac{1}{2}\,\left(F_{z,i}(a)\,\Delta u_{z,i-1}(a)\right)_k, \\
\Delta t_k &= \frac{t_{k,k-1}+t_{k+1,k}}{2},
\end{aligned} \tag{25}
$$

which are holding for 6- and 8-node volume element discretizations (Figure 11b). In the following it will be shown that also in the 3D-case through this method, good results are obtained even for non-singular, low order standard elements and rather coarse FE meshes, if the layout of the mesh around the crack front is homogeneous.

Through further generalizations of the method also the numerically more effective non-singular, higher order elements can be utilized for the fracture analysis of 2D and 3D crack problems, see Buchholz (1984, 1994); Buchholz, Wang, Lin, and Richard (1998); Buchholz, Chergui, and Dhondt (1999).

5 Case studies

In this section we present in a number of case studies detailed numerical and experimental results of the single

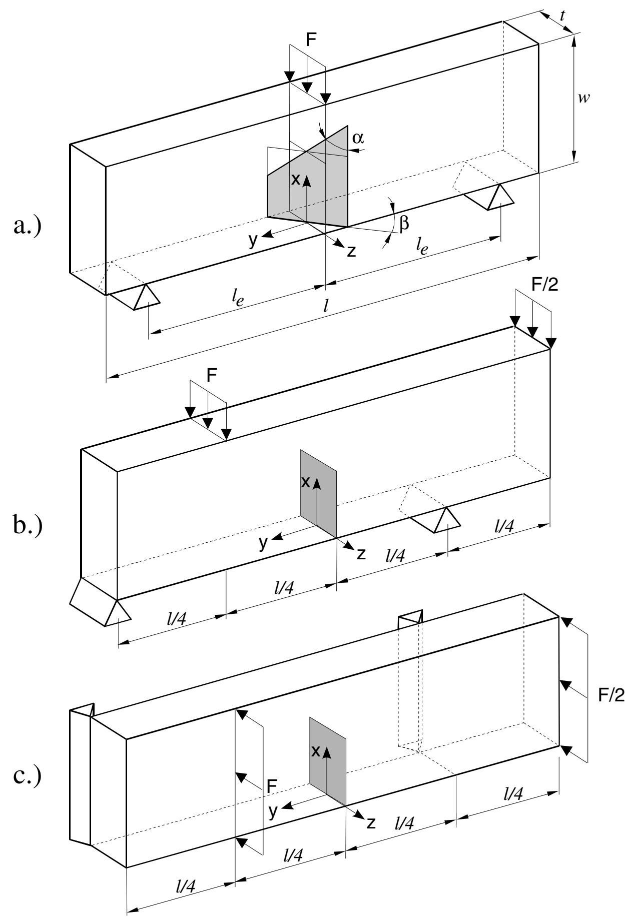

Figure 12 : SEN specimen with an inclined crack front (α) and/or inclined crack plane (β) subjected to a.) three point bending, b.) four point in-plane shear and c.) four point out-of-plane shear.

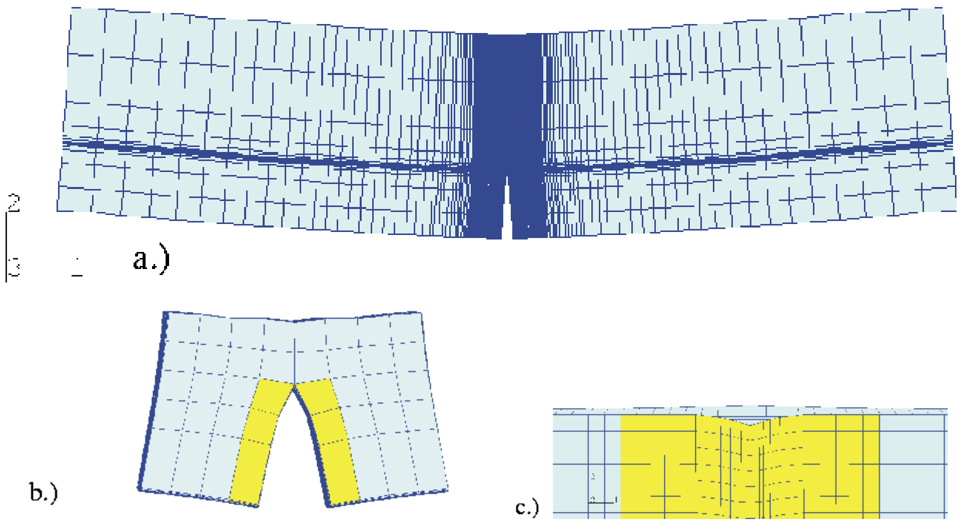

Figure 13 : Deformed FE-model of the SEN specimen with $\alpha = \beta = 90°$ subjected to 3PB. a.) Full specimen, b.) crack tip detail in front view and c.) crack tip detail in sub view.

edge notched (SEN) specimen with a normal or inclined notch plane and the following geometrical parameters: length $l = 260mm, 2l_e = 240mm$, thickness $t = 10mm$, width $w = 60mm$, norm. crack length $a/w = 1/3$, see Figure 12. The specimens are subjected to three point bending, four point in-plane shear and four point out-of-plane shear by a force $F = 2kN/mm$. In the case of three point bending, specimens with normal ($\beta = 90°$) or inclined ($\beta = 45°, 30°$) notch planes are considered.

For the three-dimensional finite element analysis the notch is considered as an already shaped crack. The MVCCI-computations are realized on a-priori refined meshes adjacent to the crack front with 6 or 8 node non-singular volume elements and about 30.000 DOFs, see for instance Figure 13a.

Related experiments are performed on specimens of transparent PMMA-material (Poisson's ratio $\nu \approx 0.3$), so that the crack front can be observed at different stages of propagation. The numerical and experimental findings are compared under special consideration of some 3D effects near the free surface with the theoretical results obtained by the asymptotical analysis.

5.1 Three point bending, straight notch plane

We consider first an SEN-specimen with $\alpha = \beta = 90°$ subjected to three point bending, see Figure 12a. Let us enforce a plane strain state in the plate by applying symmetry boundary conditions $u_z = 0$ on the two faces parallel to the x-y plane at $z/t = \pm 0.5$. The SERR in this case is expected to be constant over the crack front and equal to the corresponding G_I value obtained by a 2D plane strain analysis Murakami (1987). The results in Figure 14 show that this is the case, indeed, within an accuracy of 2%, which is sufficient for our purposes.

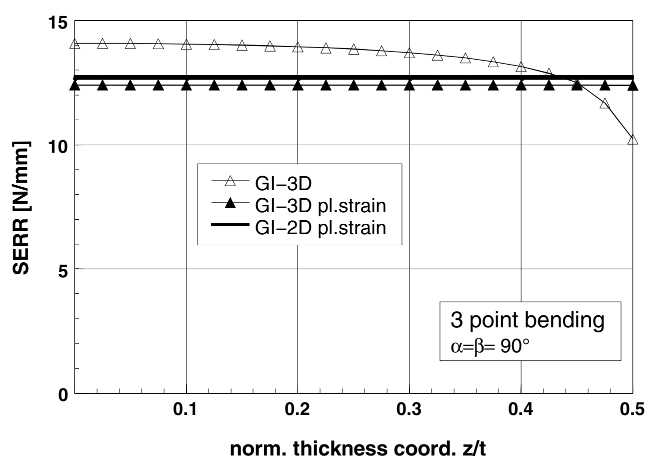

Figure 14 : SERRs versus crack front for the SEN specimen with $\alpha = \beta = 90°$ subjected to 3PB.

Next, the SEN-specimen is analyzed with stress-free boundary conditions on the plate faces. The deformed FE-model is shown in Figure 13 and corresponding results for the SERR can be found in Figure 14.

In this case G_I is about constant in the inner part of the specimen, but it is found to be distinctly higher compared with the 2D case, which means that the 2D results are not conservative. Adjacent to the free surface a well-known 3D-effect is observed, with decreasing G_I values for increasing z/t and and a stronger gradient for $z/t \rightarrow 0.5$.

The decrease of G_I for $z/t \rightarrow 0.5$ is related to the Poissons ratio and the laterally less constrained strains along the crack front adjacent to the free surface. This results in the necking of the free surface, which can be realized in a sub view on the corner, where the crack front intersects the boundary of the specimen, see Figure 13c. The understanding of this 3D-effect has also been confirmed by a further FE-analysis with Poissons ratio set to zero. In this case G_I was found to be perfectly constant all along the crack front and the related FE-model showed no necking effect at the free surfaces.

Let us analyze how this effect can be explained from theoretical point of view. In the case of a crack normal to the free surface the corresponding corner singular exponents are $\lambda_{I^*} = 0.393$ and $\lambda_{II^*} = 0.548$, see Figure 5. The third one near 1.0 is not considered, since very weak. However, due to the symmetrical loading only the symmetrical mode II^* can be excited. This mode incorporates a displacement jump over the crack faces only in y-direction, see Figure 7. Consequently $\Delta u_y \neq 0, \Delta u_x = 0, \Delta u_z = 0$ in Eq. (25) and the only non-zero SERR-component is G_I[9]. The leading order of the displacements in an asymptotical expansion is $\lambda_{II^*} = 0.548$ and, according to the concept of weak and strong singularities, this leads to G_I decreasing to zero for $z/t \rightarrow 0.5$ (weak singularity). Of course, due to a limited mesh refinement for $z/t \rightarrow 0.5$ the FE-analysis is unable to recognize the exact values in the neighborhood of a singular point at the free surface. This conclusion is confirmed by additional calculations with stronger refined meshes in z-direction, where stronger decreased G_I values for $z/t \rightarrow 0.5$ are observed. It is also in very good agreement with some recent numerical results about the SIF distribution along the crack front of a semi-circular surface crack in a plate, a quarter-circular surface crack in a bar and a corner-crack at a circular hole in a plate Han and Atluri (2002), which from asymptotical point of view should exhibit the same behavior at the free surface as the example discussed here. The numerical study in Han and Atluri (2002) is based on an alternating method, where the sub-domain with the surface crack was treated by the symmetric Galerkin-Boundary-Element-Method Han and Atluri (2003) and the uncracked global structure by FEM.

[9] Even if the notation $G_{x,y,z}$ is more appropriate for the situation around a corner the traditional notation $G_{I,II,III}$ is used in order to guarantee the compatibility with the 2D case. The SERR components $G_{I,II,III}$ should be understood here in an asymptotical sense.

The above named necking effect at the free surface for Poisson's ratios $\nu \neq 0$ is also exactly predicted by the asymptotical analysis: The trace of mode II^* on the free surface in Figure 7 shows clearly some non-zero z-displacements, which result in a surface necking, whereas for $\nu = 0$ this z-displacements vanish (Figure 8), so that the necking effect should disappear too. Moreover, for $\nu = 0$ the mode II^* is completely identical to the plane strain mode I, so that a perfectly constant G_I distribution along the crack front is expected, exactly as observed.

In a related experiment the development of a typically curved crack front with retarded crack growth adjacent to the free surfaces is observed, as can be expected due to the shape of the G_I distribution, Figure 15.

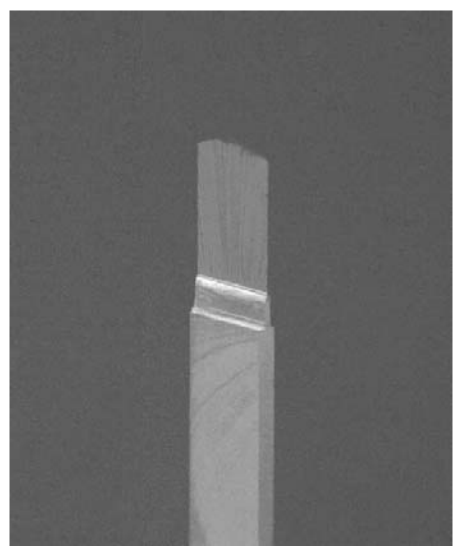

Figure 15 : Curved, fatigued crack front with $\alpha \approx 101°$ of the cracked SEN specimen with $\beta = 90°$ subjected to 3PB.

The angle under which the propagating crack intersects the free surface is slightly obtuse, which corresponds well to the critical angle of $\alpha \approx 101°$ for $\beta = 90°$, see Figure 6.

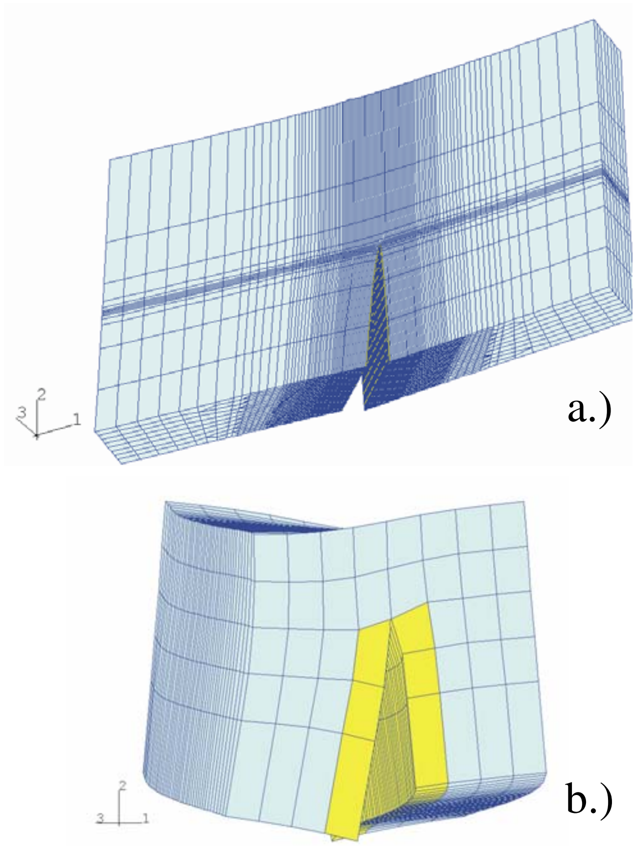

Figure 16 : Deformed FE-model of the SEN specimen with $\alpha = 90°$ and $\beta = 45°$ subjected to 3PB. a.) Center part of the full specimen, b.) crack tip detail in front view.

This is in very good agreement with the result in Reference Bazant and Estenssoro (1979).

5.2 Three point bending, inclined notch plane

Next, a SEN specimen with $\alpha = 90°$ and an inclined notch plane ($\beta = 45°$) subjected to three point bending is considered, see Figure 12a. In this case, not only mode I but also mode III loading conditions are generated, due to the inclined notch plane, as can be realized in the deformed FE-model in Figure 16.

As a reference, the problem of an inclined crack in an infinite elastic space with a simple tension far field σ_0 can be used. The corresponding SIFs are given by $k_I = \sigma_0\sqrt{\pi a}\sin^2\beta$ and $k_{III} = \sigma_0\sqrt{\pi a}\sin\beta\cos\beta$, which gives a ratio $k_{III}/k_I = 1$ for $\beta = 45°$ Pook (1993).

The results of the MVCCI calculations for the SEN specimen are plotted in Figure 17. In the inner part of the

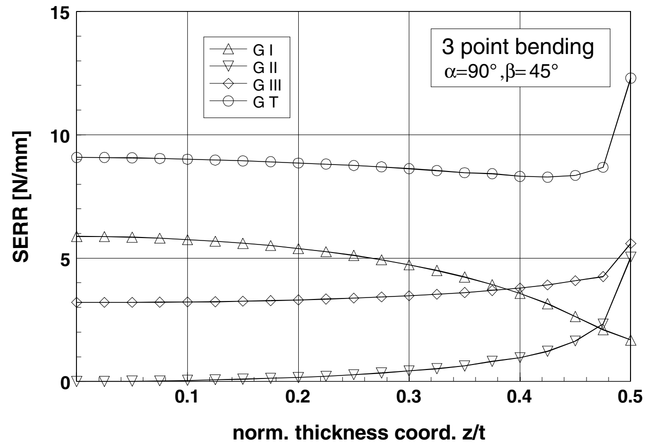

Figure 17 : SERRs versus crack front for the SEN specimen with $\alpha = 90°$ and $\beta = 45°$ subjected to 3PB.

specimen G_I, G_{III} are found to be nearly constant, but with a ratio $G_{III}/G_I \approx 0.5$ and for $z/t > 0.25$ the SERR G_I decreases distinctly, whereas G_{III} increases. Furthermore the 3D-analysis by the MVCCI-method shows that also mode II loading conditions are induced locally, due to a strong mode coupling effect between mode III and II. Moreover, G_{II} shows remarkably increasing values for $z/t \rightarrow 0.5$. The corresponding deformation of the specimen can be seen in Figure 16a and in the crack tip detail given in Figure 16b. In particular, considerable mode-II or in-plane sliding displacements of the crack faces can be realized in Figure 16b, in addition to the expected crack opening and out-of-plane sliding displacements. These results are also in very good agreement with the numerical analysis of the SIF distribution along the crack front of an inclined semi-circular surface crack in a plate Han and Atluri (2002), which from asymptotical point of view should exhibit the same behavior at the free surface as the example discussed here.

One could mean now, the decreasing G_I values toward the free surface are expected, due to the global bending moment distribution in the specimen — for the type of loading presented here the bending moment is maximal in the middle of the specimen ($y = 0$) and decreases for $|y| > 0$. One could also mean, that the observed G_{II} values at the free surface are related to the shear effect of the loading. Additional investigations on a SEN specimen under *four*-point bending[10] have shown, however,

[10] In the case of *four*-point bending *two* forces are applied symmetrically with respect to the *x*-*z* plane, in contrast to the *three*-point

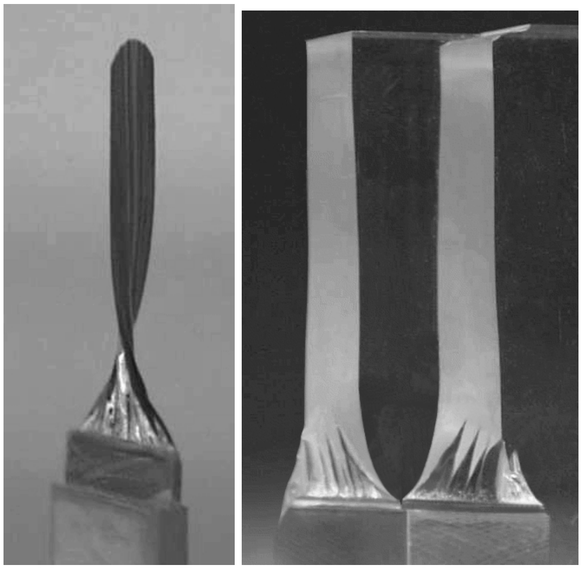

Figure 18 : Cracked SEN specimen with $\alpha = 90^\circ$ and $\beta = 45^\circ$ subjected to 3PB. View of the crack at a certain stage of propagation (left) and both parts of a fully cracked specimen with facets (right).

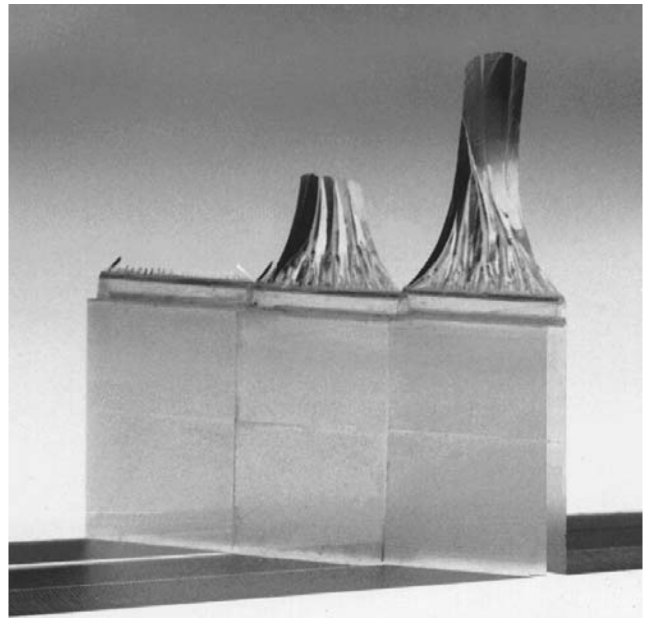

Figure 19 : Cracked SEN specimens with $\alpha = 90^\circ$ and $\beta = 45^\circ$ subjected to 3PB at three different stages of crack propagation.

that the same phenomena are observed in the case of a constant bending moment and a vanishing shear effect also, so that some global loading arguments cannot explain the SERR distribution in Figure 17.

From the asymptotical point of view, the two singular exponents for this case are $\lambda_{I^*} = 0.388$ and $\lambda_{II^*} = 0.676$. Since no special symmetry is present both modes are excited and the leading order of the displacements in the neighborhood of the free surface is $\lambda_{I^*} = 0.388$, which corresponds to a strong singularity. Mode I^* incorporates jumps in both U_x and U_z over the crack faces, i.e. $\Delta u_x \neq 0, \Delta u_z \neq 0$ in Eq. (25), which results in G_{II}, G_{III} as non-zero components of the SERR and therefore suggest a "combination" of modes II and III at the free surface. The strong singularity $\lambda_{I^*} = 0.388$ causes increasing values of G_{II}, G_{III} for $z/t \to 0.5$ as expected, whereas the weak-singular mode II^* results in decreasing G_I-values with $z/t \to 0.5$, exactly as observed in Figure 17. In Figure 18 the strong impact of these locally varying mixed mode loading conditions on the crack shape at a certain stage of propagation can be realized. On a macro scale the crack twists off its original plane, due to the locally effective G_I, G_{II} values, see Figure 18 left. On a meso scale the crack surface of the twisted crack is not smooth, in particular at the beginning of crack growth, but reveals narrow facets forming some angle ϕ with the direction of the overall crack growth, see Figure 18 right. They are likely to be caused by the locally effective G_{III} values and have also been observed and discussed by Pook Pook (1995). The facet angle can approximately be given by

$$\tan 2\phi = \frac{2k_{III}}{k_I(1-2\nu)}, \tag{26}$$

according to Pook (1995). Here the facets are connected with some irregular cliffs and merge at some later stage of propagation, Figure 19. However, this may not be always the case, as can be seen in Figure 20, where the same experiment for a SEN-specimen with $\beta = 30^\circ$ is shown: The separate cracks, which were initiated at the free-surface corners of the original crack front have not merged yet and may also not merge at a later stage of crack propagation.

In both cases, the crack growth starts[11] at the free surface as expected, see Figures 19 and 20.

bending, where only *one* force in the *x*-*z* plane is used.

[11] Even if this seems to be a problem of a local *onset* and not of an ex-

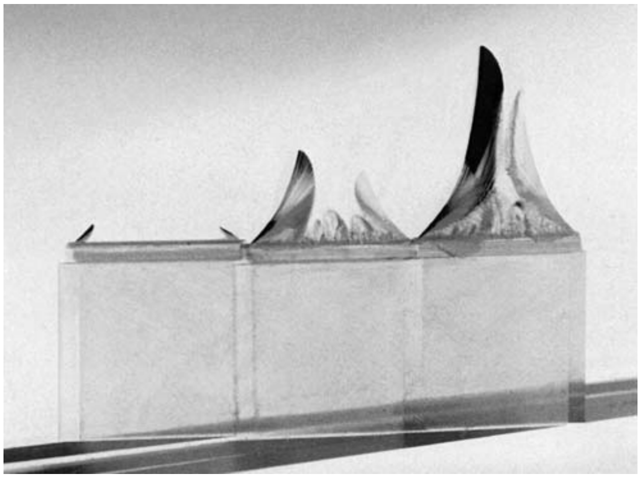

Figure 20 : Cracked SEN specimens with $\alpha = 90^\circ$ and $\beta = 30^\circ$ subjected to 3PB at three different stages of crack propagation.

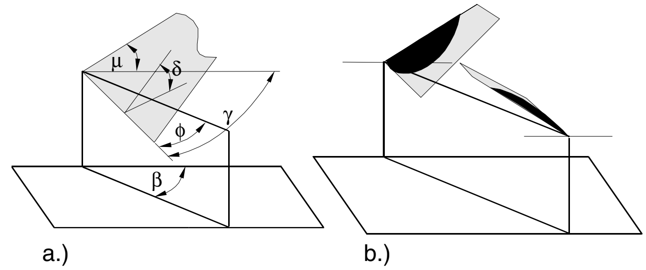

Figure 21 : a.) Geometrical relations and b.) expected shape and orientation of crack growth at the point, where a new crack is initiated near the free surface of a SEN specimen with an inclined notch plane subjected to 3PB.

The facet angle at the boundary can be obtained from Eq. (26) assuming $k_{III}/k_I = \infty$, which results in $\phi = 45^\circ$ and a new crack plane, which is normal to the free surface (original notch plane $\beta = 45^\circ$). Simultaneously, the crack plane kinks off from the original direction of propagation due to the locally effective G_I, G_{II} values, as already mentioned. Applying the Maximum-SERR criterion Nuismer (1975); Richard (1985) and assuming $k_I/k_{II} = 0$ at the corner a kink-off angle of 70° is obtained, as in the case of pure mode II loading. The above geometrical relations $\gamma = 90^\circ, \delta = 90^\circ - 70^\circ = 20^\circ$ are illustrated in Figure 21. With a new crack plane, which is normal to the free surface, a crack front termination angle $\alpha \approx 68^\circ$ is expected, see Figure 6. The visible angle μ of the crack path at the free surface coincides here with $\delta = 20^\circ$. A good agreement with the experimental observation in Figures 19 and 18 can be realized.

In the case of an original notch plane of $\beta = 30^\circ$ the situation is slightly more complicated. The inclination angle β of the new crack plane with respect to the free surface can be calculated by the simple geometrical relation

$$\cos\beta = \cos\gamma \sin\delta, \tag{27}$$

tension, using the concept for predicting crack nucleation on sharp notches proposed in Leguillon (2001), very similar results can be obtained. Within this approach the problem of the local onset is handled in a very similar way as a crack extension by replacing the crack SIF by a notch stress concentration factor. The concept of strong and weak singularities still remains true.

where $90^\circ - \delta$ denotes the kink-off angle and γ the facet angle with respect to the free surface. In the case of $\gamma = 75^\circ$ and $\delta = 20^\circ$ the new crack plane will have $\beta \approx 85^\circ$ and again a crack front termination angle $\alpha \approx 68^\circ$ is expected. Moreover, the visible angle μ of the crack path at the free surface, see Figure 21, should be

$$\tan\mu = \sin\gamma \tan\delta, \tag{28}$$

which results in $\mu \approx 19.5^\circ$ for our case. Both, the termination angle $\alpha \approx 68^\circ$ and $\mu \approx 19.5^\circ$ agree well with the experimental observation, see Figure 20.

5.3 *Four point in-plane shear*

The next case to be considered is the SEN-specimen subject to four point in-plane shear loading (Figure 12b), which results in the deformed FE-model shown in Figure 22. In this case the generated G_{II} values are rather constant in the inner part of the specimen, see Figure 23, but for $z/t > 0.4$ they increase remarkably, which means again that the corresponding 2D results are not conservative. Furthermore the detailed 3D-analysis by the MVCCI-method shows that also mode III loading conditions are induced locally, although the external loading of the SEN-specimen does not contain any out-of-plane shear component.

In Buchholz, Chergui, and Richard (2001b) the appearance of G_{III} is interpreted as a weak mode coupling effect between mode II and mode III, which is related to Poisson's ratio and the laterally less constrained strains adjacent to the free surface. Thus, this effect is distinct for $z/t \to 0.5$, but less pronounced more inside the specimen and vanishes for $z/t = 0$. In the front view of the

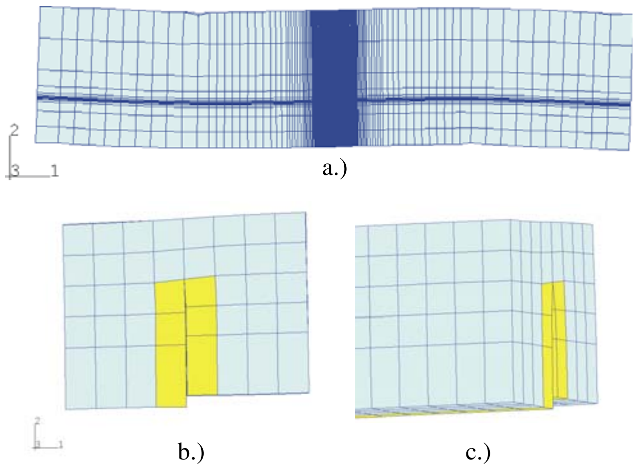

Figure 22 : Deformed FE-model of the SEN specimen with $\alpha = \beta = 90°$ subjected to in-plane 4PS. a.) Full specimen, b.) crack tip detail in front view and c.) crack tip detail in axionometric view.

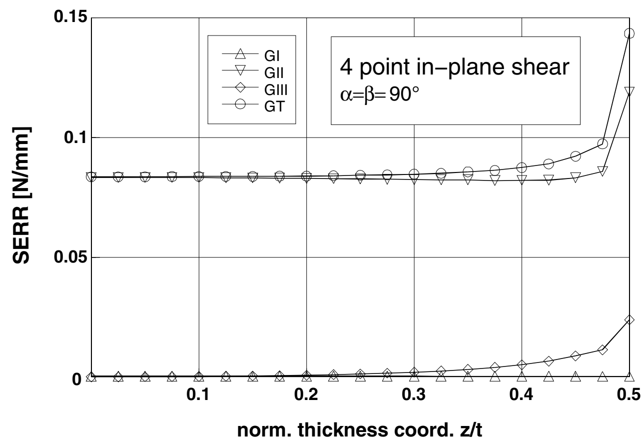

Figure 23 : SERRs versus crack front for the SEN specimen with $\alpha = 90°$ and $\beta = 90°$ subjected to in-plane 4PS.

deformed crack tip detail of the specimen (Figure 22b) clearly the generated in-plane sliding displacements of the crack faces can be seen, but in the axionometric view of the same crack tip detail (Figure 22c) also the small induced out-of-plane sliding displacements can be realized at the corner where the crack front intersects the free surface. The interpretation and understanding of this effect is confirmed again by a further FE-analysis with Poisson's ratio set to zero Buchholz, Chergui, and Richard (2001a). In this case G_{II} was found to be perfectly constant along the crack front and G_{III} was found to vanish completely.

From the asymptotical point of view the in-plane shear loading (anti-symmetrical with respect to the notch plane) cannot excite the symmetrical mode II^* at the surface and therefore the only singular mode which is present is mode I^*, with the corresponding singular exponent $\lambda_{I^*} = 0.393$. This mode incorporates for $\nu \neq 0$ both displacement jumps in x and z-direction (Figure 7), which results in $G_{II}, G_{III} \neq 0$ at the free surface, so that this effect is interpreted as a coupling between mode II and III. The resulting strong singular behavior is manifested in strongly increasing values of G_{II}, G_{III}, however as already discussed, the numerics only leads to finite values at the free surface. For $\nu = 0.0$ mode I^* is equivalent to the plain strain mode II, see Figure 8 bottom, so that in this case G_{II} should be constant along the crack front, whereas G_{III} should disappear, exactly as observed.

Because the above named mode coupling effect is related to the Poisson's ratio, it does not influence further crack growth considerably ("weak" coupling). This is confirmed by experimental findings for the SEN-specimen under in-plane 4PS loading conditions for unstable crack growth. Due to the generated predominant G_{II} loading conditions along the crack front, the crack kinks off from the initial crack (or notch) plane and the experimentally observed kink-angle is constant along the crack front and appears hardly to be influenced by the discussed weak coupling effect between mode II and III: No shear lips or facets can be observed, in spite of mode III. Consequently this case can be considered as a plane problem approximately, so that the kink-off angle can be predicted by the well established maximum SERR Nuismer (1975); Richard (1985) or the maximum tangential stress criterion Erdogan and Sih (1963); Richard (1985) resulting in a value of $\approx 70°$ for the case of pure mode II loading with $k_I/k_{II} = 0$.

This has been confirmed also through detailed experimental studies on the compact tension shear (CTS) specimen Richard (1981, 1985) with an initial mode I precrack ($\alpha = \beta = 90°$) subjected to pure in-plane shear loading, in combination with a special loading device Richard and Benitz (1983); Richard (1985), which covers the full range of in-plane mixed mode loadings. The observed crack growth at an early stage of crack propagation is shown in Figure 24, where an interesting effect

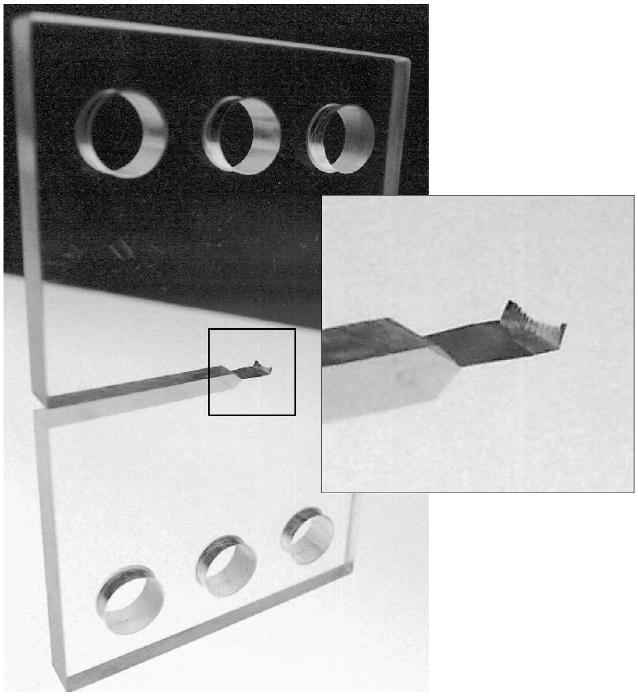

Figure 24 : Cracked CTS specimen with $\alpha = \beta = 90°$ and a mode I pre-crack subjected to in-plane shear.

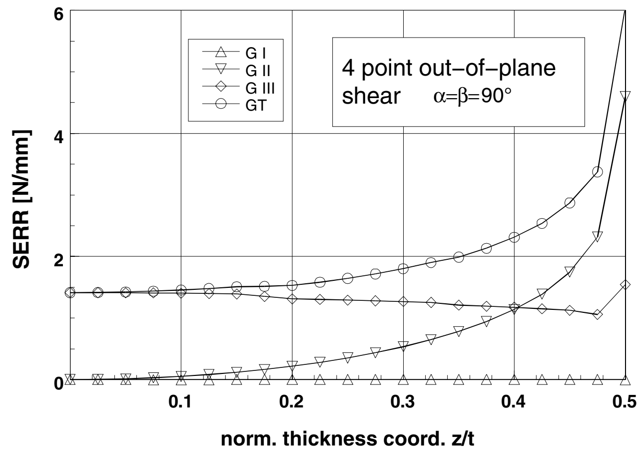

Figure 26 : SERRs versus crack front for the SEN specimen with $\alpha = \beta = 90°$ subjected to out-of-plane 4PS.

can be seen at the crack front near to the free surface.

Since the termination angle of the mode I pre-crack is $101°$ (see Figure 6), an inclination angle $\beta = 86°$ of the new crack can be calculated by Eq. (27) with $\gamma = 180° - 101° = 79°$ and $\delta = 90° - 70° = 20°$. The new crack is not in pure mode I and the in-plane shear component of the loading excites the mode I^* at the corner. The strong singularity results in an early crack propagation adjacent to the free surface. The acute crack termination angle, which is realized in Figure 24, corresponds well to the theoretically expected critical value of $\alpha \approx 68°$ for $\beta = 86°$, Figure 6.

5.4 Four point out-of-plane shear

Finally, the out-of-plane shear loading of the SEN-specimen is considered (Figure 12c), which results in the deformed FE-model of the specimen as shown in Figure 25.

In this case the generated G_{III} values are about constant and predominant along the crack front for $z/t < 0.4$, see Figure 26.

The component G_{III} only increases for $z/t \rightarrow 0.5$. But furthermore for $z/t > 0.25$ also the remarkably increasing mode II loading conditions are analyzed by the MVCCI-method. In Buchholz, Chergui, and Richard (2001b) they are understood to be locally induced along the crack front through a strong mode coupling effect between mode III and II, which was found to be not related to Poisson's ratio, but to the global deformation behavior of the specimen. This has been confirmed again by Buchholz, Chergui, and Richard (2001a), where in the case $\nu = 0$ the G_{III} values decrease slightly, but the G_{II} curve is *not* affected. In the front view of the deformed crack tip detail of the specimen (Figure 25b) clearly the generated out-of-plane sliding displacements of the crack faces can be seen, but in the axionometric view (Figure 25c) also the induced and in this case considerably great in-plane sliding displacements of the crack faces are obvious.

From the asymptotical point of view, only mode I^* with $\lambda_{I^*} = 0.393$ is excited, due to the out-of-plane shear loading. This mode incorporates both jumps in x and z-direction, which is interpreted as coupling between mode II and III. The resulting strong-singular behavior is manifested in strongly increasing values of G_{II}, G_{III}, however, as already discussed, the numerics only leads to a finite value at the free surface.

In the corresponding experiment these loading conditions along the crack front result in the very interesting crack growth behavior which is shown in Figure 27. As one could expect from the locations of the maximum values of the total SERR G_T at the upper and lower free surface

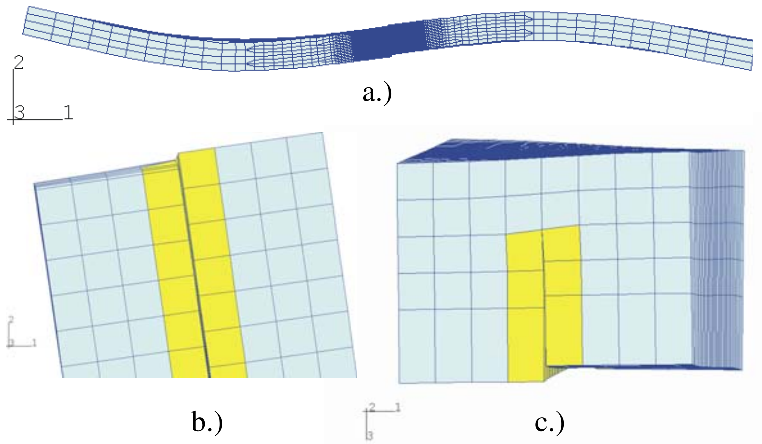

Figure 25 : Deformed FE-model of the SEN specimen with $\alpha = \beta = 90°$ subjected to out-of-plane 4PS. a.) full specimen, b.) crack tip detail in front view and c.) crack tip detail in axionometric view.

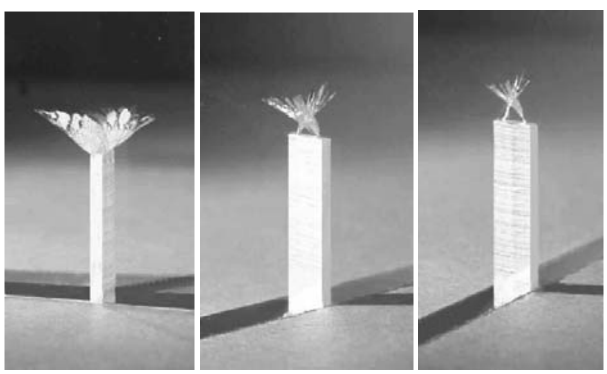

Figure 27 : Cracked SEN specimen with $\alpha = \beta = 90°$ subjected to out-of-plane 4PS seen from different sides and viewpoints.

of the specimen ($z/t = \pm 0.5$) two separate cracks are observed to initiate. The planes in which the cracks start to grow appear to be governed by the generated mode III loading conditions and have an anti-symmetric orientation with respect to the planes of symmetry of the specimen. An approximation of the angle with the initial notch plane can again be found by Eq. (26), see Pook (1995). Assuming $k_{III}/k_I = \infty$, $\phi = 45°$ is obtained. The kink-off from the initial propagation direction appear to be strongly affected by the mode II loading conditions. By the Maximum-SERR criterion Nuismer (1975); Richard (1985) a kink-off angle of 70° is again obtained, assuming $k_I/k_{II} = 0$. With $\gamma = 45°$ and $\delta = 20°$ an inclination angle $\beta = 76°$ is obtained from Eq. (27), which corresponds to a crack front termination angle $\alpha \approx 68°$, Figure 6. Even if a measurement of this angle is not possible, due to the very irregular crack shape, an acute angle seems to appear, which qualitatively agrees with the expected value. However, the angle $\mu = 14.5°$ of the crack path at the free surface, which is expected from Eq. (28) with $\gamma = 45°$ and $\delta = 20°$ cannot be confirmed, the experimentally observed angle seems to be greater. Figure 27 shows the two separate cracks at a certain stage of crack growth from different sides and viewpoints.

6 Conclusion

In the present work the problem of an surface-breaking crack with straight or inclined crack plane has been analyzed from the asymptotical, numerical and experimental point of view. With the software presented in Section 3 first the asymptotical expansion of the solution has been constructed for arbitrary inclined crack shapes near the point where the crack terminates on the free surface. With respect to this point we can conclude

- The stress state there is three-dimensional and up to four singular modes $I^* - IV^*$ exist, which are in general independent of the plain strain modes I,II,III.
- The state there is not plane stress.
- The state there is not plane strain, except for $\alpha = \pi/2, \beta = \pi/2, \nu = 0.0$, where mode II^* corresponds to mode I and mode I^* corresponds to mode II. Mode III^* is not equivalent to mode III, even for $\nu = 0.0$.

- Based on the theory of 3D corner singularities it is not appropriate to speak about “mode coupling” effects between mode II and III. The corner mode I^* only exhibits jumps in the displacement components U_x, U_z and therefore suggests a “combination” of mode II,III.

Furthermore, by the concept of weak and strong singularities the asymptotics of the usual fracture parameters SIF and SERR in the neighborhood of the corner point have been obtained. This allows the use of a convenient single parameter description of failure also for the surface-breaking crack problem. Moreover, we can conclude that:

- Near a corner point the SIF and SERR will in general tend either to zero or to infinity.
- This asymptotics hides the incompatibility of the 2D and 3D modes.
- A crack which propagates self-similarly cannot have an arbitrarily shape, but will take a crack front termination angle, at which the corner singularity is equal to the edge one. This angle has been determined for arbitrary inclined crack planes.
- If a numerical analysis is performed on a “wrong” geometry, i.e. not exactly on that, which a propagating crack would have, the corner influence will still be present and will affect the accuracy of the numerical results.
- Mode II^* (mode I) is not always the critical mode, as often assumed. For a wide range of crack front termination angles mode II^* is weak-singular at the corner point, whereas mode I^* (mode II/III) is strong-singular, so that the latter will control fracture at early propagation stages.

And finally we can conclude: Even if the region at which the crack termination point dominates is small, it can be the *critical* zone in which crack propagation takes place first. A conservative approach to fracture of solids can be guaranteed only by a reasonable consideration of all relevant three-dimensional effects.

References

Bazant, Z.; Estenssoro, L. (1979): Surface singularity and crack propagation. *International Journal of Solids and Structures*, vol. 15, pp. 405–426.

Buchholz, F.-G. (1984): Improved formulae for the finite element calculation of the strain energy release rate by the modified crack closure integral method. In Robinson, J.(Ed): *Accuracy, Reliability and Training in FEM Technology*, pp. 650–659. Robinson and Associates.

Buchholz, F.-G. (1994): Finite element analysis of a 3d mixed-mode fracture problem by virtual crack closure integral methods. In Krishna Murthy, A.; Buchholz, F.-G.(Eds): *Fracture Mechanics. Proc. of the Indo-German Workshop on Advances in Fracture Mechanics*, pp. 7–12, Bangalore, India. Interline Publ., Bangalore, 1994.

Buchholz, F.-G.; Chergui, A.; Dhondt, G. (1999): A comparison of SIF and SERR results with reference solutions regarding 3D and mode coupling effects for different specimens. In Aliabadi, M.(Ed): *Fracture and Damage Mechanics 99*, London.

Buchholz, F.-G.; Chergui, A.; Richard, H. (2001): Computational fracture analysis by the MVCCI-method regarding 3D and mode coupling effects for different specimens and loading conditions. In de Freitas, M.(Ed): *Proc. of the 6th Int. Conf. on Biaxial/Multiaxial Fatigue & Fracture, Vol. II*, pp. 991–998, Lisboa, Portugal.

Buchholz, F.-G.; Chergui, A.; Richard, H. (2001): Fracture analyses and experimental results on crack growth under general mixed mode loading conditions. In Guagliano, M.; Aliabadi, M.(Eds): *Advances in fracture and damage mechanics II. Proc. of the 2nd Int. Conf. on fracture and damage mechanics*, pp. 451–456, Milan, Italy. Hoggar, Geneva, 2001.

Buchholz, F.-G.; Grebner, H.; Dreyer, K.-H.; Krome, H. (1988): 2D- and 3D-applications of the improved and generalized modified crack closure integral method. In Atluri, S.; Yagawa, G.(Eds): *Computational Mechanics. Proc. of the Int. Conf. on Comp. Eng. Sci. (ICES 88) Vol. I*, pp. 14.i.1–14.i.4, Atlanta, Georgia, USA. Springer, New York, 1988.

Buchholz, F.-G.; Wang, H.; Lin, J.; Richard, H. (1998): 3D finite-element-analysis of different test specimens for investigations on mixed mode I, II and III fracture. In *Computational Mechanics. CD-ROM Proc. of the 4th World Congr. on Comp. Mech. (WCCM IV)*, pp. 1–21, Part III, Section 4, Paper 1, Buenos Aires, Argentina.

Costabel, M.; Dauge, M.; Duduchava, R. (2001): Asymptotics without logarithmic terms for crack problems. Prépublication 01-50, Institut de Recherche Mathématique de Rennes, France, 2001.

Dauge, M. (1988): *Elliptic Boundary Value Problems on Corner Domains. Smoothness and Asymptotics of Solutions*. No. 1341 in Lecture notes in mathematics. Springer, Berlin.

Dauge, M. (2000): "Simple" corner-edge asymptotics. Internet publication, http://www.maths. univ-rennes1.fr/∼dauge/publis/corneredge.pdf, 2000.

Dhondt, G.; Chergui, A.; Buchholz, F.-G. (2001): Computational fracture analysis of different specimens regarding 3D and mode coupling effects. *Engineering Fracture Mechanics*, vol. 68, pp. 383–401.

Dimitrov, A.; Andrä, H.; Schnack, E. (2001): Efficient computation of order and mode of corner singularities in 3D - elasticity. *International Journal for Numerical Methods in Engineering*, vol. 52, pp. 805–827.

Dimitrov, A.; Andrä, H.; Schnack, E. (2002): Singularities near three-dimensional corners in composite laminates. *International Journal of Fracture*, vol. 115, pp. 361–375.

Dimitrov, A.; Schnack, E. (2002): Asymptotical expansion in non-Lipschitzian domains — a numerical approach. *Numerical Linear Algebra with Applications*, vol. to appear.

Erdogan, F.; Sih, G. (1963): On the crack extension in plates under plane loading and transverse shear. *J. Basic Engng*, vol. 85, pp. 519–525.

Ghahremani, F. (1991): A numerical variational method for extracting 3D singularities. *International Journal of Solids and Structures*, vol. 27, pp. 1371–1386.

Grisvard, P. (1992): *Singularities in Boundary Value Problems*. No. 22 in Recherches en Mathématiques Appliquées. Masson, Springer, Paris.

Han, Z.; Atluri, S. (2002): SGBEM (for cracked local subdomain) – FEM (for uncracked global structure) alternating method for analyzing 3D surface cracks and their fatigue-growth. *CMES: Computer Modeling in Engineering & Sciences*, vol. 3, pp. 699–716.

Han, Z.; Atluri, S. (2003): Truly meshless local petrov-galerkin (MLPG) solutions of traction & displacement BIEs. *CMES: Computer Modeling in Engineering & Sciences*, vol. 4, pp. 665–678.

He, M.; Hutchinson, J. (2000): Surface crack subjected to mexed mode loading. *Engineering Fracture Mechanics*, vol. 65, pp. 1–14.

Irwin, G. (1957): Analysis of stresses and strains near the end of a crack traversing a plate. *Journal of Applied Mechanics*, vol. 24, pp. 361–364.

Kassir, M.; Sih, G. (1975): *Mechanics of Fracture 2 — Three Dimensional Crack Problems*. Noordhoff, Leyden.

Kondratiev, V. (1967): Boundary problems for elliptic equations in domains with conical or angular points. *Transact. Moscow Math. Soc.*, vol. 16, pp. 227–313.

Kozlov, V.; Maz'ya, V.; Rossmann, J. (1997): *Elliptic Boundary Value Problems in Domains with Point Singularities*. No. 52 in Mathematical Surveys and Monographs. AMS.

Krishnamurthy, T.; Rammamurthy, T.; Vijayakumar, K.; Dattaguru, B. (1985): Modified crack closure integral method for higher order finite elements.. In Kant, T.(Ed): *Finite Elements in Computational Mechanics*, pp. 891–900. Pergamon Press, Oxford.

Leguillon, D. (1993): Asymptotic and numerical analysis of a crack branching in non-isotropic materials. *European Journal of Mechanics, A/Solids*, vol. 12, pp. 33–51.

Leguillon, D. (1995): Computation of 3D singularities in elasticity. In Costabel, M.; Dauge, M.; Nicaise, S.(Eds): *Boundary Value Problems and Integral Equations in Nonsmooth Domains*, no. 167 in Lecture Notes in Pure and Applied Mathematics, pp. 161–170. Dekker, New York. Proc. of the Conf. at the CIRM, Lumini, May 3-7 1993.

Leguillon, D. (2001): A criterion for crack nucleation at a notch in homogeneous materials. *C.R.Acad.Sci.Paris*, vol. Série IIb 329, pp. 97–102.

Leguillon, D.; Sanchez-Palencia, E. (1987): *Computation of Singular Solutions in Elliptic Problems and Elasticity*. Masson, Wiley, Paris.

Leguillon, D.; Sanchez-Palencia, E. (1992): Fracture in heterogeneous materials. Weak and strong singularities. In Ladaveze, P.; Zienkiewicz, O.(Eds): *New advances in Computational Structural Mechanics*, pp. 423–434. Elsevier.

Leguillon, D.; Sanchez-Palencia, E. (1999): On 3D cracks intersecting a free surface in laminated composites. *International Journal of Fracture*, vol. 99, pp. 25–40.

Mazja, V.; Nasarow, S.; Plamenewski, B. (1991): *Asymptotische Theorie elliptischer Randwertaufgaben in singulär gestörten Gebieten*. Mathematische Lehrbücher und Monographien: 2. Abteilung. Akademie-Verlag.

McKellar, D.; Tait, R.; Douglas, A. (1997): FEM determination of stress intensity distrubution for semi-elliptical flaws in bending. In Reddy, B.(Ed): *Recent developments in computational and applied mechanics*, pp. 227–236. CIMNE, Barcelona.

Murakami, Y. (1987): *Stress intensity factors handbook*. Pergamon, Oxford.

Nuismer, R. (1975): An energy release rate criterion for mixed mode fracture. *International Journal of Fracture*, vol. 11, pp. 245–250.

Panasyuk, V.; Andrejkiv, A.; Stadnik, M. (1981): Three-dimensional static crack problem solutions (a review). *Engineering Fracture Mechanics*, vol. 14, pp. 245–260.

Pook, L. (1993): A finite element analysis of the angle crack specimen. In Rossmanith, H.; Miller, K.(Eds): *Mixed-Mode Fatigue and Fracture*, pp. 285–302. Mechanical Engineering Publ.

Pook, L. (1994): Some implications of corner point singularities. *Engineering Fracture Mechanics*, vol. 48, pp. 367–378.

Pook, L. (1995): On fatigue crack paths. *International Journal of Fatigue*, vol. 17, pp. 5–14.

Richard, H.-A. (1981): A new compact shear specimen. *International Journal of Fracture*, vol. 17, pp. R105–R107.

Richard, H.-A. (1985): *Bruchvorhersagen bei überlagerter Normal- und Schubbeanspruchung von Rissen*. No. 631 in VDI-Forschungsheft. VDI-Verlag, Düsseldorf.

Richard, H.-A.; Benitz, K. (1983): A loading device for the creation of mixed mode in fracture mechanics. *International Journal of Fracture*, vol. 22, pp. R55–R58.

Rybicki, E.; Kanninen, M. (1977): A finite element calculation of stress intensity factors by a modified crack closure integral. *Engineering Fracture Mechanics*, vol. 9, pp. 931–938.

Sih, G. (1971): A rewiev of the three-dimensional stress problem for a cracked plate. *International Journal of Fracture Mechanics*, vol. 7, pp. 39–61.

v. Petersdorff, T. (1989): *Randwertproblem der Elastizitätstheorie für Polyeder-Singularitäten und Approximation mit Randelementmethoden*. PhD thesis, Technische Hochschule Darmstadt, 1989.

Westergaard, H. (1939): Bearing pressures and cracks. *Journal of Applied Mechanics*, vol. 61, pp. A49–53.

Williams, M. (1957): On the stress distribution at the base of a stationary crack. *Journal of Applied Mechanics*, vol. 24, pp. 109–114.